Copy No. 6

[redacted]

RM No. A9C21

~~1153~~
~~672~~
9,12

NACA RM No. A9C21

RESEARCH MEMORANDUM

AERODYNAMIC STUDY OF A WING-FUSELAGE COMBINATION EMPLOYING A WING SWEPT BACK 63°. - EFFECTS OF SPLIT FLAPS, ELEVONS, AND LEADING-EDGE DEVICES AT LOW SPEED

By Edward J. Hopkins

Ames Aeronautical Laboratory
Moffett Field, Calif.

CLASSIFICATION CHANGED
UNCLASSIFIED

To ______
By authority of Nasa Res. Ab. + RN-113 Date 3-14-57
NB 4-4-57

FOR REFERENCE

NOT TO BE TAKEN FROM THIS ROOM

CLASSIFIED DOCUMENT

This document contains classified information affecting the National Defense of the United States within the meaning of the Espionage Act, USC 50:31 and 32. Its transmission or the revelation of its contents in any manner to an unauthorized person is prohibited by law. Information so classified may be imparted only to persons in the military and naval services of the United States, appropriate civilian officers and employees of the Federal Government who have a legitimate interest therein, and to United States citizens of known loyalty and discretion who of necessity must be informed thereof.

NATIONAL ADVISORY COMMITTEE
FOR AERONAUTICS
WASHINGTON
May 19, 1949

[redacted]

NACA RM No. A9C21

NASA Technical Library
3 1176 01434 4742

NATIONAL ADVISORY COMMITTEE FOR AERONAUTICS

RESEARCH MEMORANDUM

AERODYNAMIC STUDY OF A WING-FUSELAGE COMBINATION EMPLOYING A WING SWEPT BACK 63°.– EFFECTS OF SPLIT FLAPS, ELEVONS, AND LEADING-EDGE DEVICES AT LOW SPEED

By Edward J. Hopkins

SUMMARY

An investigation was conducted to evaluate the effects of split flaps, elevons, sharp leading edges, drooped-nose flaps, and extended-nose flaps on the lift, drag, and pitching-moment characteristics at low speed of a wing-fuselage combination having a wing with the leading edge swept back 63° and having an aspect ratio of 3.5. Measurements were also made of the rolling moments produced by the elevons. In addition, a study was made to evaluate the effects of the fuselage and possible Reynolds number effects on the characteristics of the wing.

The optimum chordwise position of the split flap for increasing the lift coefficient attained before the occurrence of longitudinal instability and for reducing the drag at high lift coefficients was the position with the split flap hinge line coincident with the trailing edge of the wing. The effectiveness of the elevons for producing rolling moments was nearly constant up to an angle of attack of 9°, but decreased at greater angles of attack. The full-span leading-edge flaps increased the lift coefficient attained before the occurrence of longitudinal instability considerably more than did the 50-percent span leading-edge flaps. The extended-nose flap was about twice as effective as the drooped-nose flap in reducing the drag of the model at the higher lift coefficients.

INTRODUCTION

A coordinated program is being conducted at Ames Aeronautical Laboratory to provide information throughout an extensive range of Mach and Reynolds numbers on a wing-fuselage combination employing

[redacted]

a wing with the leading edge swept back 63° and having an aspect ratio of 3.5. According to the theoretical considerations of reference 1, a wing of this plan form should be capable of efficient flight at supersonic Mach numbers up to 1.5. Experimental results from tests of wings of this plan form at high Mach or Reynolds numbers are presented in references 2, 3, and 4.

A wing-fuselage combination having a wing of the plan form just described was investigated in one of the Ames 7- by 10-foot wind tunnels to evaluate the effectiveness of various flaps and particularly their capacity for eliminating the large changes in the longitudinal stability which have been found to occur above a lift coefficient of 0.4 (reference 4). In this connection, a drooped-nose flap and an extended-nose flap were tested in conjunction with trailing-edge flaps. Furthermore, an investigation was made to determine the optimum chordwise position of split flaps and the effectiveness of elevons of two different plan forms.

NOTATION

All forces and moments are referred to the wind axes with the origin on an extension of the wing root chord at the same longitudinal position as a point at 25 percent of the wing mean aerodynamic chord.

C_D	drag coefficient $\left(\frac{\text{drag}}{qS}\right)$
C_L	lift coefficient $\left(\frac{\text{lift}}{qS}\right)$
C_l	rolling-moment coefficient $\left(\frac{\text{rolling moment}}{4qSb}\right)$
C_m	pitching-moment coefficient $\left(\frac{\text{pitching moment}}{qS\bar{c}}\right)$
A	aspect ratio $\left(\frac{2b^2}{S}\right)$
b	span of semispan wing perpendicular to the plane of symmetry, feet
c	wing chord parallel to plane of symmetry, feet

[redacted]

$\bar{c}$	mean aerodynamic chord $\left(\dfrac{\int_0^b c^2\,dy}{\int_0^b c\,dy}\right)$, feet
l_w	wing loading, pounds per square foot
q	free-stream dynamic pressure $\left(\frac{1}{2}\rho V^2\right)$, pounds per square foot
R	Reynolds number $\left(\frac{V\bar{c}}{\nu}\right)$
r	fuselage radius, feet
S	area of semispan wing, square feet
V	free-stream velocity, feet per second
V_s	sinking speed, feet per second
x	longitudinal distance, feet
y	lateral distance, feet
α	angle of attack of the wing chord plane, degrees
δ	control-surface deflection measured in a plane normal to the hinge line (For positive deflections, the flap is below the wing-chord plane.), degrees
ν	kinematic viscosity of air, feet squared per second
ρ	mass density of air, slugs per cubic foot

Subscripts

d	drooped-nose flap
e	elevon

[redacted]

f	split flap
i	induced
n	extended-nose flap
u	uncorrected

CORRECTIONS

An explanation of the method used in calculating the wind-tunnel-wall corrections which were applied to the data is given in the appendix. The equations used in correcting the data are as follows:

$$C_D = C_{D_u} + 0.0319 \ C_{L_u}{}^2$$

$$C_L = 0.99 \ C_{L_u}$$

$$C_l = 0.938 \ C_{l_u}$$

$$C_m = C_{m_u} + 0.0010 \ C_{L_u}$$

$$\alpha = \alpha_u + 1.36 \ C_{L_u} + 0.19 \ (C_{L_u})_{\delta=0^\circ}$$

Measurements were made of the deflection due to the aerodynamic loads of the model at various spanwise positions and of the change in angle of attack of the wing tip for dynamic pressures ranging from 20 to 150 pounds per square foot. For a lift coefficient of 0.35 and a dynamic pressure of 50 pounds per square foot the wing tip deflected 0.33 inch above its no-load position; however, only a negligible change in angle of attack of the wing tip was measured. Evidence that the effects of model distortion were negligible was also obtained from tests of this model in the Ames 12-foot pressure wind tunnel (reference 3) at dynamic pressures of 53 and 105 pounds per square foot for a constant Reynolds number of 9.75×10^6. Only small effects on the aerodynamic characteristics of the wing were produced by this dynamic-pressure variation. Hence, no corrections have been applied to the data of the present tests for the effects of model distortion.

MODEL AND TESTS

The semispan wing used for this investigation had its leading edge swept back 63°, an aspect ratio of 3.5 based on the geometry of the complete wing, a taper ratio (ratio of tip chord to root chord) of 0.25, no twist, no dihedral, and the NACA 64A006 profile parallel to the plane of symmetry. The model wing is shown in figure 1 mounted from the floor of the Ames 7- by 10-foot wind tunnel No. 2. Model dimensions are presented in figure 2.

A gap of one-eighth inch existed between the turntable and the extension of the wing spar which passed through the turntable to support the model. The clearance between the tunnel floor and the model was about one-quarter inch except near the nose of the long fuselage where the gap was about three-quarters inch.

The fuselage used in part of this investigation was semicircular in cross section and had a fineness ratio of 12.5. This fuselage is hereafter referred to as the long fuselage.[1] Due to possible effects of the wind-tunnel walls on the experimental results, the maximum angle of attack employed with this fuselage was 26°. To allow for a greater angle-of-attack range for the major portion of the investigation, this fuselage was shortened to a fineness ratio of 10.5. This fuselage is referred to as the short fuselage.[2] The wing is shown in combination with the long and short fuselages in figure 3.

The model was tested with a 0.25-chord split flap in four chordwise positions on the wing with hinge lines along lines of constant-percent wing chord (40, 60, 75, and 100 percent of the

---

[1] Equation for contour of long fuselage (see fig. 2)

$$r = 0.680\left[1.000 - \left(1.000 - \frac{x}{8.500}\right)^2\right]^{3/4}$$

[2] Equations for contour of short fuselage (see fig. 2)

$$\text{Nose:}\quad r = \sqrt{77.371 - (x-3.116)^2} - 8.226$$

$$\text{Tail:}\quad r = \sqrt{0.918 - (x-0.718)^2} - 0.635$$

The ordinates of the center portion of the short fuselage were identical to the ordinates of the center portion of the long fuselage from 51.00 inches to 183.60 inches from the nose of the long fuselage.

[redacted]

wing chord), and in two chordwise positions with hinge lines normal to the air stream. The model was also investigated with a split flap of triangular plan form with its hinge line coincident with the trailing edge of the wing. All of the split flaps had the same area and extended from the fuselage to the midsemispan of the wing. The dimensions and positions of the split flaps on the wing are shown in figure 4.

The model was investigated with an elevon having chords equal to 25 percent of the local wing chord, and with an elevon of constant chord. Both elevons extended from the midsemispan to the wing tip and had unsealed radius noses. The dimensions of the elevons are given in figure 2.

Sectional views of the leading-edge flaps and the sharp leading edge are shown in figure 5. The model was tested with these devices having span equal to 50 and 100 percent of the wing span. The 50-percent-span leading-edge flaps extended from the midsemispan to the wing tip; whereas the 50-percent-span sharp leading edge extended from the midsemispan to the wing-fuselage juncture. Photographs of the model with the full-span drooped-nose and extended-nose flaps are shown in figure 6.

Most of the tests were conducted at a dynamic pressure of 50 pounds per square foot which corresponded to a Reynolds number of 4.2 million. However, to investigate possible dynamic scale effects, some tests were performed throughout a Reynolds number range of 2.5 to 7.2 million.

RESULTS AND DISCUSSION

Plain Wing and Wing-Fuselage Combinations

The results of tests of the plain wing and wing-fuselage combinations are presented in figure 7. The following characteristics of the plain wing are noted just above a lift coefficient of 0.2: (1) The rate of change of lift with angle of attack increased, and (2) the aerodynamic center shifted rearward. Observations of the flow in the boundary layer, by means of short tufts of thread attached to the wing surface, indicated that a local region of flow separation occurred near the wing leading edge in the vicinity of the wing tip at a lift coefficient of approximately 0.2. The following characteristics of the plain wing are noted in figure 7 just above a lift coefficient of 0.4: (1) The rate of change of lift with angle of attack decreased, (2) the wing efficiency factor, $\frac{dC_L^2}{dC_{D_i}} \times \frac{1}{\pi A}$, decreased, and (3) the aerodynamic center shifted forward. The surface tufts indicated a complete breakdown of flow near the wing tip at a lift coefficient of about 0.4.

The addition of either fuselage increased the lift-curve slope $(\partial C_L/\partial \alpha)$ from 0.042 to 0.046 per degree and increased the drag at low lift coefficients. The same increase of the lift-curve slope was measured for a geometrically similar model, having a full-span wing, in the Ames 40- by 80-foot wind tunnel (reference 4). The wing in combination with the short fuselage had the same general characteristics as the wing in combination with the long fuselage except for slight differences in the pitching moments. During the investigation of the various control devices, the short fuselage was used in combination with the wing to permit testing up to an angle of attack of 38°.

Reynolds Number

Most of the data in this report were obtained at a Reynolds number of 4.2 million; however, to investigate possible dynamic-scale effects the data presented in figure 8 were obtained throughout a Reynolds number range of 2.5 to 7.2 million. Increasing the Reynolds number from 2.5 to 4.2 million increased the lift coefficient attained before the occurrence of longitudinal instability of the wing with the long fuselage from about 0.4 to 0.5, but had a negligible effect on this lift coefficient of the plain wing. However, a further increase of Reynolds number to 7.2 million resulted in no improvement of this lift coefficient. The drag coefficients were reduced slightly for all lift coefficients between 0.1 and 0.8, but the lift-curve slope was not greatly affected by increasing the Reynolds number from 2.5 to 7.2 million.

Split Flaps

The effect of the 0.25-chord split flap in several chordwise positions on the characteristics of the model is shown in figure 9. The split flap with its hinge line at the trailing edge of the wing yielded the largest increment of lift coefficient for all angles of attack and flap deflections investigated (an increment of at least 0.4 up to an angle of attack of 24°) and increased the lift coefficient attained before the occurrence of longitudinal instability from about 0.5 to 0.8. As the hinge line of the split flap was moved forward from 100 to 40 percent of the wing chord, the flap effectiveness decreased rapidly. Although the split flap with its hinge line at the wing trailing edge produced the largest lift increases, this flap also produced the largest changes in longitudinal balance.

The split flaps with their hinge lines normal to the air stream provided less negative pitching moments and smaller lift increments than did the split flap with its hinge line at the trailing edge of the wing (fig. 9(a)). With the split flap deflected 60° in the forward position with its hinge normal to the air stream the lift coefficient attained before the occurrence of longitudinal instability was increased from about 0.5 to 0.6. Surface tufts indicated that the split flaps with their hinge lines normal to the air stream caused flow separation to occur initially near the midsemispan of the wing at an angle of attack of 0°. At angles of attack greater than 12°, these split flaps caused a larger portion of the wing to stall, which is probably responsible for the decreased lift-curve slope and the decreased maximum lift coefficient (fig. 9 (a)).

Increase of the deflection of the split flaps from 45° to 75° caused relatively small changes in the lift and pitching-moment characteristics (fig. 9(a)). Deflecting some of the split flaps more than 45°, for example, the flap hinged at 100 percent of the wing chord, decreased the maximum lift coefficient. Only the split flap at the trailing edge of the wing greatly reduced the drag of the model at high lift coefficients (fig. 9(b)).

The data for the model with the split flap of triangular plan form and with the split flap of constant-percent chord (both hinged along the wing trailing edge) are presented in figure 10. At high angles of attack the split flap of triangular plan form produced slightly larger increments of lift coefficient than the split flap of constant-percent chord of the same area. Longitudinal instability occurred at approximately the same lift coefficient with the same deflection of either flap, but the split flap of triangular plan form deflected 45° produced slightly less negative pitching moments at small angles of attack. With either flap at 0° angle in the extended position, the lift-curve slope was increased from 0.046 to 0.052 per degree and the aerodynamic center was shifted rearward 1.5 percent of the mean aerodynamic chord at small lift coefficients.

The drag characteristics of the model with the triangular flap were similar to those of the model with the 25-percent-chord split flap for the same flap deflections (fig. 10(b)).

Elevons

The characteristics of the model with various deflections of the constant-percent-chord elevon and the constant-chord elevon are presented in figure 11. The pitching moments with the constant-chord elevon undeflected were slightly different from the pitching moments with the constant-percent-chord elevon undeflected. Similar discrepancies may be found in other figures of this report. These discrepancies are believed to have been caused by small differences in the contour or in the 0° settings of the various controls. At small angles of attack, the rates of change of pitching- and rolling-moment coefficients with elevon deflection for the two elevons were approximately in proportion to their area moments about the pitch or roll axes.[s] The rate of change of lift, pitching-moment, and rolling-moment coefficient with elevon deflection remained nearly constant up to an angle of attack of 9°, decreased between angles of attack of 9° and 17°, but increased at higher angles of attack for negative deflection of the elevons. In the low lift range, the rate of change of pitching-moment and rolling-moment coefficients with elevon deflection decreased as the negative deflection of the elevon exceeded 30°.

The characteristics of the model with the constant-chord elevon and the 0.25-chord split flap deflected 45° at the wing trailing edge are presented in figure 12. This was the elevon split-flap combination tested with the leading-edge flaps which will be discussed in the succeeding sections of this report. The rate of change of lift and rolling-moment coefficients with elevon deflection remained nearly constant to an angle of attack of 5°, but decreased at higher angles of attack. Therefore, with the split flap the effectiveness of the constant-chord elevon began to decrease at a smaller angle of attack than without the split flap (figs. 11 and 12).

As mentioned hereinbefore the split flap hinged at the wing trailing edge produced large changes in balance; therefore, the longitudinal-stability margin should be considered in choosing the type of control surface to be used for balance. With the negative deflection of the elevon limited to 40°, the split flap deflected 45° and the center of gravity at $0.25\bar{c}$, the wing-fuselage combination could be balanced only for lift coefficients up to 0.46 (fig. 12). However, it appears possible to use a more rearward center of gravity and still to maintain adequate longitudinal stability at the lower lift coefficients. With a more rearward center of gravity, the wing-fuselage combination could be balanced at all lift coefficients with smaller elevon deflections, thus allowing more elevon effectiveness for lateral control.

---

[s] The moment of the area of the constant-chord elevon about either the pitch or the roll axis was approximately 1.5 times that of the constant-percent-chord elevon.

Leading-Edge Devices

The model was tested with both the drooped-nose flap and the extended-nose flap deflected 30°, 35°, 40°, and 50°. The optimum deflection for either flap was found to be about 40°. As only slight differences were noted in the results for the several deflections, only the results for the 40° deflection are presented. The model was also investigated with each of the leading-edge flaps in various combinations with the constant-chord elevon undeflected and deflected negatively 20°, and the 0.25-chord split flap undeflected and deflected 45° at the trailing edge of the wing.

The characteristics of the model with the drooped-nose flap of 50-percent wing span and of full wing span are presented in figures 13 and 14, respectively. The drooped-nose flap of 50-percent wing span decreased the lift at all angles of attack and failed to improve the pitching-moment characteristics of the model (fig. 13). However, the drooped-nose flap of full wing span gave slightly better results, increasing the lift coefficient at which longitudinal instability occurred about 0.15 with the split flap retracted and about 0.04 with the split flap extended (fig. 14). With the elevon deflected -20°, the split flap deflected 45°, and the drooped-nose flap of full wing span deflected 40°, the lift coefficient attained before the occurrence of longitudinal instability was greater than 1.0 (fig. 14).

The characteristics of the model with the extended-nose flap of 50-percent wing span and full wing span are presented in figures 15 and 16, respectively. The extended-nose flap of 50-percent wing span proved to be as ineffective as the drooped-nose flap of 50-percent wing span for increasing the lift coefficient of the model before the occurrence of longitudinal instability (figs. 13 and 15). However, with the split flap deflected 45° and the elevon deflected -20°, the extended-nose flap produced a more nearly linear variation of pitching-moment coefficient with lift coefficient up to a lift coefficient of 0.9 than did the drooped-nose flap (figs. 13 and 15). With the split flap deflected 45°, the extended-nose flap of full wing span increased the lift coefficient attained before instability more than did the drooped-nose flap of full wing span, but shifted the aerodynamic center forward about 9 percent of the mean aerodynamic chord (figs. 14 and 16). This forward shift of the aerodynamic center due to the extended-nose flap of full wing span was partly alleviated by deflecting the elevon −20° (the elevon caused a rearward displacement of the aerodynamic center of 3 percent of the mean aerodynamic chord (fig. 16)).

The drag characteristics of the model with the full-span leading-edge flaps are presented in figure 17. The drooped-nose flap or the extended-nose flap of full wing span reduced the drag coefficients of the model at high lift coefficients, with the split flap either retracted or extended. The extended-nose flap was about twice as effective as the drooped-nose flap in reducing the drag at high lift coefficients.

The importance of drag at high lift coefficients can be appreciated by considering the sinking speed of an airplane. The variation of lift coefficient with drag coefficient for sinking speeds of 20, 30, and 40 feet per second for an assumed wing loading of 40 pounds per square foot is presented in figure 17. It should be observed that at a lift coefficient of 1.0 the full-span extended-nose flap would decrease the sinking speed of the wing-fuselage combination with the split flap deflected 45° at the wing trailing edge from greater than 40 feet per second to about 30 feet per second. The limiting value of sinking speed recommended in reference 5 is 25 to 30 feet per second.

The characteristics of the model with the sharp leading edges of 50-percent wing span and of full wing span are shown in figure 18. The sharp leading edges eliminated the increase in longitudinal stability which occurred just above a lift coefficient of 0.3; however, they decreased the lift coefficient attained before the occurrence of longitudinal instability. The addition of the sharp leading edges moved the aerodynamic center forward at low lift coefficients and increased slightly the lift at high angles of attack.

Highest Lift Coefficient Attained Before Longitudinal Instability

Although none of the devices eliminated the longitudinal instability, some devices substantially increased the lift coefficient at which instability first occurred. The highest lift coefficients attained before the occurrence of longitudinal instability for the model with the various flaps are summarized in figure 19. The largest gain in this lift coefficient was produced by the split flap deflected 45° at the trailing edge of the wing. The addition of the leading-edge flaps of 50-percent wing span deflected 40° increased this lift coefficient slightly. However, with either of the leading-edge flaps of full wing span deflected 40°, the elevon deflected -20°, and the split flap deflected 45°, a lift coefficient greater than 1.0 was attained before longitudinal instability occurred.

CONCLUSIONS

From an experimental investigation at low speed of the effects of split flaps, elevons, and leading-edge devices on the characteristics of a wing-fuselage combination employing a wing swept back 63° it is concluded that:

1. For the plain wing-fuselage combination, an increase of Reynolds number from 2.5 to 4.2 million increased the lift coefficient attained before the occurrence of longitudinal instability from about 0.4 to 0.5, but a further increase of Reynolds number to 7.2 million resulted in no improvement of this lift coefficient.

2. The optimum chordwise position of the split flap for delaying the occurrence of longitudinal instability to a higher lift coefficient was the position with the flap hinge line coincident with the wing trailing edge. This was the only position of the split flap which greatly reduced the drag of the model at the higher lift coefficients.

3. The rate of change of lift, pitching moment, and rolling moment with elevon deflection remained nearly constant up to an angle of attack of about 9°, but decreased at greater angles of attack.

4. The 50-percent-span leading-edge flaps gave no significant improvement in the pitching-moment characteristics of the model. However, the full-span leading-edge flaps deflected 40° increased the lift coefficient attained before the occurrence of longitudinal instability to a value greater than 1.0 with the split flap deflected 45° at the trailing edge of the wing and the elevon deflected -20°.

5. The extended-nose flap of full wing span was about twice as effective as the drooped-nose flap of full wing span in reducing the

drag of the model at the higher lift coefficients.

6. With the full-span extended-nose flap deflected 40°, the split flap deflected 45° at the trailing edge of the wing, and a wing loading of 40 pounds per square foot, a sinking speed of 30 feet per second was indicated for a lift coefficient of 1.0.

Ames Aeronautical Laboratory,
National Advisory Committee for Aeronautics,
Moffett Field, Calif.

APPENDIX

WIND-TUNNEL-WALL CORRECTIONS

Wind-tunnel-wall corrections for unswept reflection-plane models mounted on a 7-foot wall of a 7- by 10-foot wind tunnel have been presented in reference 6. For the purpose of the present report, the method used in reference 6 was modified to include the effects of sweepback upon the tunnel-wall corrections for a reflection-plane model mounted on a 10-foot wall.

The spanwise distribution of load was approximated by using two staggered horseshoe vortices as shown in figure 20. The normal method of summing the induced velocities of a doubly infinite image pattern was then followed. The induced velocity at the point P was computed separately for each horseshoe vortex and added in the following manner:

$$\left[\left(\frac{w}{\Gamma}\right)_1\right]_{x=x'} + \left[\left(\frac{w}{\Gamma}\right)_2\right]_{x=x''} - \left[\left(\frac{w}{\Gamma}\right)_1\right]_{x=x''} = \left(\frac{w}{\Gamma}\right)_P$$

(The subscript 1 refers to the horseshoe vortex having the trailing vortex a distance y_1' from the plane of symmetry, and the subscript 2 refers to the horseshoe vortex having the trailing vortex a distance y_1'' from the plane of symmetry (fig. 20).)

The total boundary-induced vertical velocity was then

$$\frac{w}{\Gamma} = \frac{1}{4\pi}\sum_{n=-\infty}^{\infty}\sum_{m=-\infty}^{\infty}(-1)^m\left\{\frac{2na-y_1-y}{(2na-y_1-y)^2+(mh)^2}\left[1+\frac{x}{\sqrt{(2na-y_1-y)^2+x^2+(mh)^2}}\right]\right.$$

$$-\frac{2na+y_1-y}{(2na+y_1-y)^2+(mh)^2}\left[1+\frac{x}{\sqrt{(2na+y_1-y)^2+x^2+(mh)^2}}\right]+\frac{x}{x^2+(mh)^2}\left[\frac{2na-y_1-y}{\sqrt{(2na-y_1-y)^2+x^2+(mh)^2}}\right.$$

$$\left.\left.-\frac{2na+y_1-y}{\sqrt{(2na+y_1-y)^2+x^2+(mh)^2}}\right]\right\}$$

where

a	7-foot dimension of wind tunnel
h	10-foot dimension of wind tunnel
m	number of image patterns in the Z direction
n	number of image patterns in the Y direction
$\frac{w}{\Gamma}$	boundary-induced vertical velocity

The remaining symbols in the above equation are defined in figure 20.

The values of $\frac{W}{F}$ calculated by the above equation were then used in the basic equation given in reference 6 to obtain the actual wind-tunnel-wall corrections listed in a previous section of this report.

REFERENCES

1. Jones, Robert T.: Estimated Lift-Drag Ratios at Supersonic Speed. NACA TN No. 1350 1947.

2. Madden, Robert T.: Aerodynamic Study of a Wing-Fuselage Combination Employing a Wing Swept Back 63°.– Characteristics at a Mach Number of 1.53 Including Effect of Small Variations of Sweep. NACA RM No. A8J04, 1949.

3. Reynolds, Robert M., and Smith, Donald W.: Aerodynamic Study of a Wing-Fuselage Combination Employing a Wing Swept Back 63°.– Subsonic Mach and Reynolds Number Effects on the Characteristics of the Wing and on the Effectiveness of an Elevon. NACA RM No. A8D20, 1948.

4. McCormack, Gerald M., and Walling, Walter C.: Aerodynamic Study of a Wing-Fuselage Combination Employing a Wing Swept Back 63°.– Investigation of a Large-Scale Model at Low Speed. NACA RM No. A8D02, 1949.

5. Gustafson, F. B., and O'Sullivan, William J., Jr.: The Effect of High Wing Loading on Landing Technique and Distance, with Experimental Data for the B-26 Airplane. NACA ARR No. L4K07, 1945.

6. Swanson, Robert S., and Toll, Thomas A.: Jet-Boundary Corrections for Reflection-Plane Models in Rectangular Wind Tunnels. NACA Rep. No. 770, 1943.

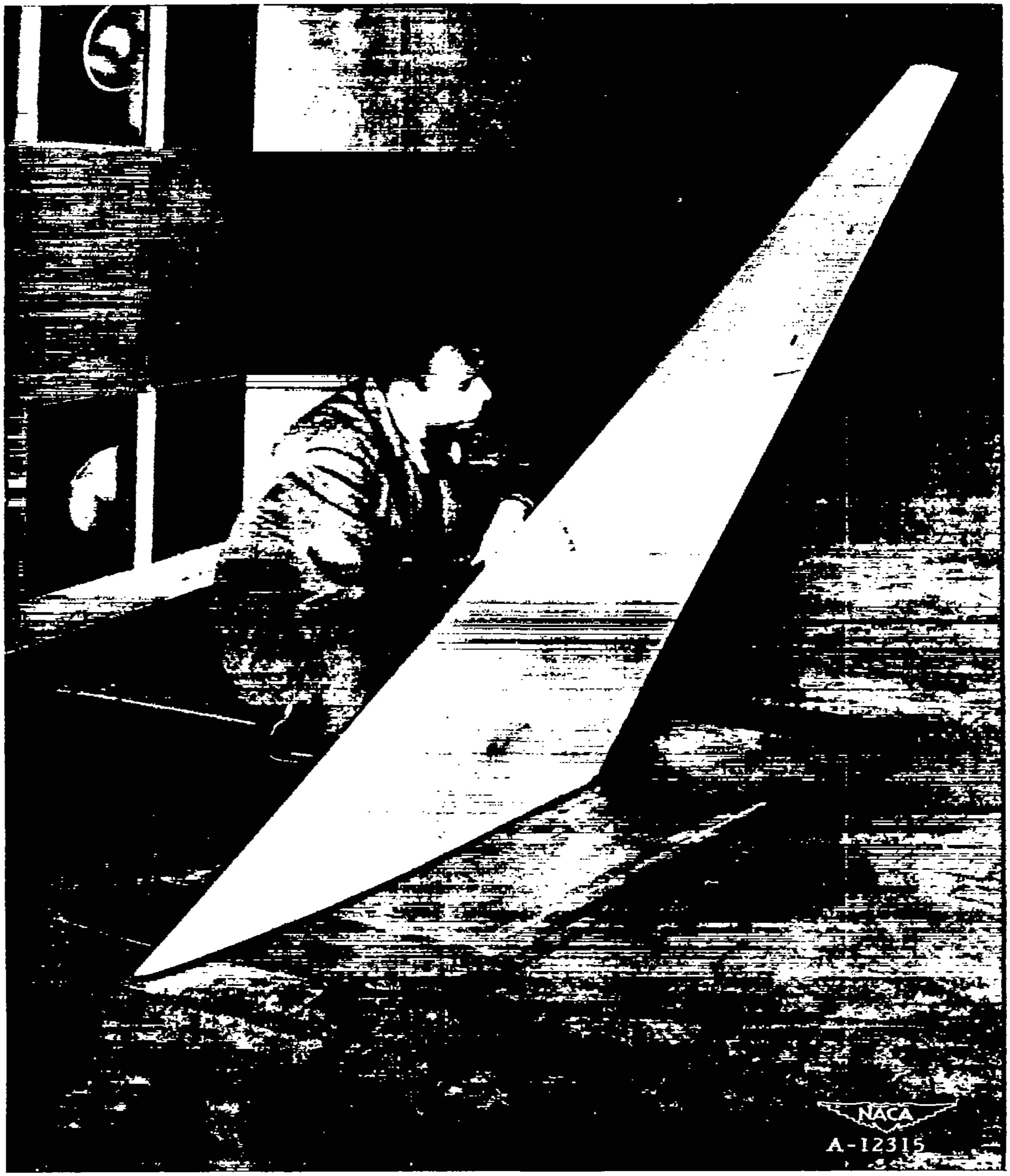
NACA
A-12315

Figure 1.– The wing mounted in one of the Ames 7– by 10–foot wind tunnels.

[redacted]

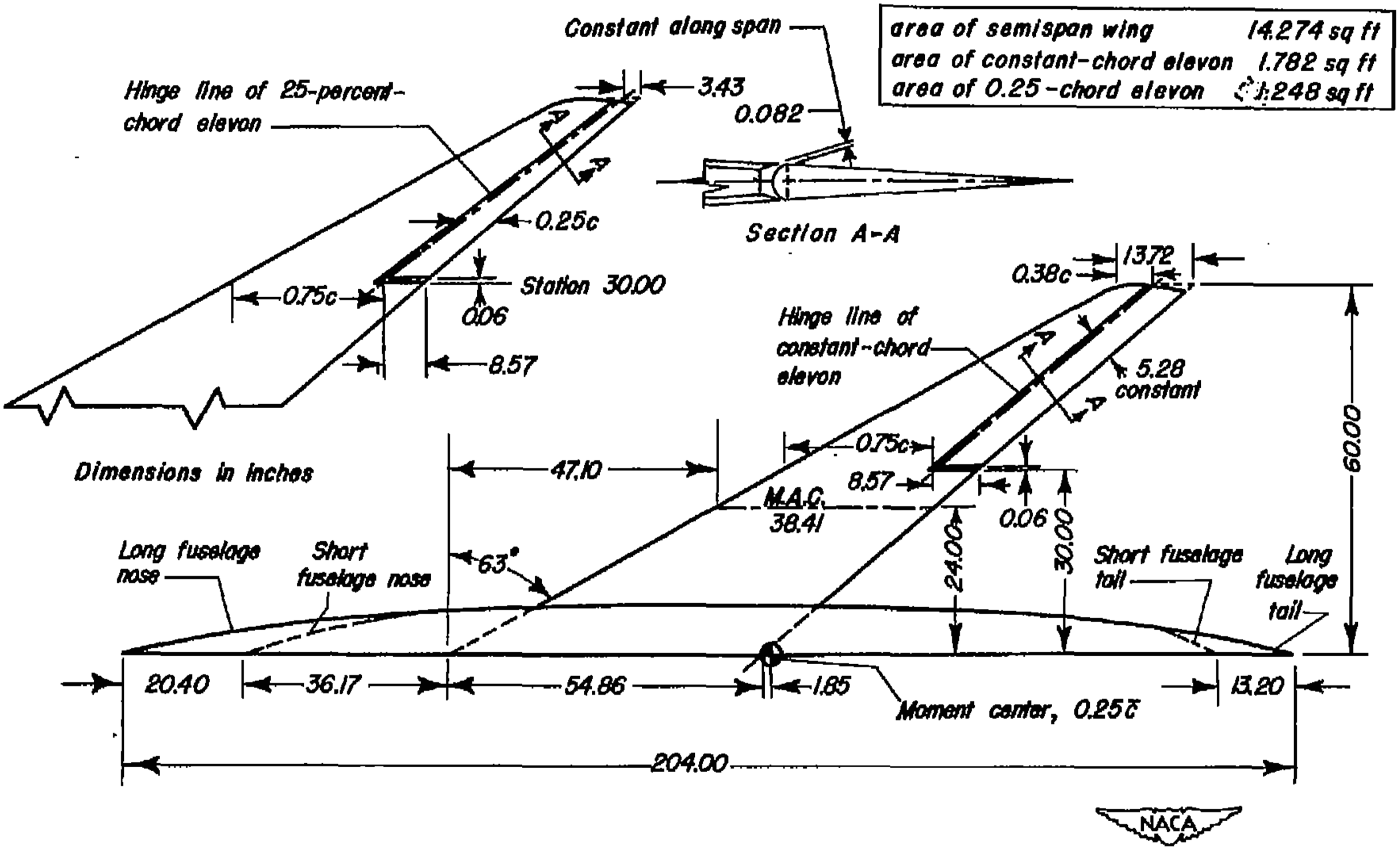
Constant along span
Hinge line of 25-percent-chord elevon
3.43
0.082
area of semispan wing 14.274 sq ft
area of constant-chord elevon 1.782 sq ft
area of 0.25-chord elevon 1.248 sq ft
A
A
0.25c
Section A-A
0.75c
Station 30.00
0.06
8.57
13.72
0.38c
Hinge line of constant-chord elevon
A
A
5.28 constant
Dimensions in inches
0.75c
47.10
8.57
M.A.C. 38.41
0.06
24.00
30.00
60.00
63°
Long fuselage nose
Short fuselage nose
Short fuselage tail
Long fuselage tail
20.40
36.17
54.86
1.85
Moment center, 0.25c̄
13.20
204.00
NACA

Figure 2.- The model geometry.

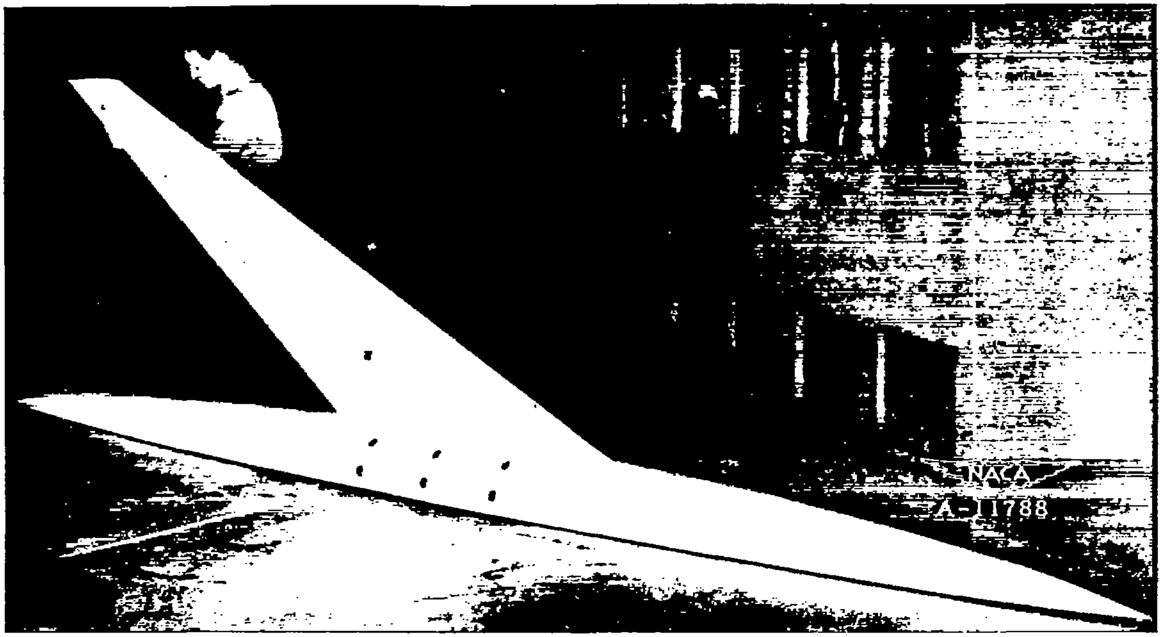
NACA
A-11788

(a) Long fuselage.

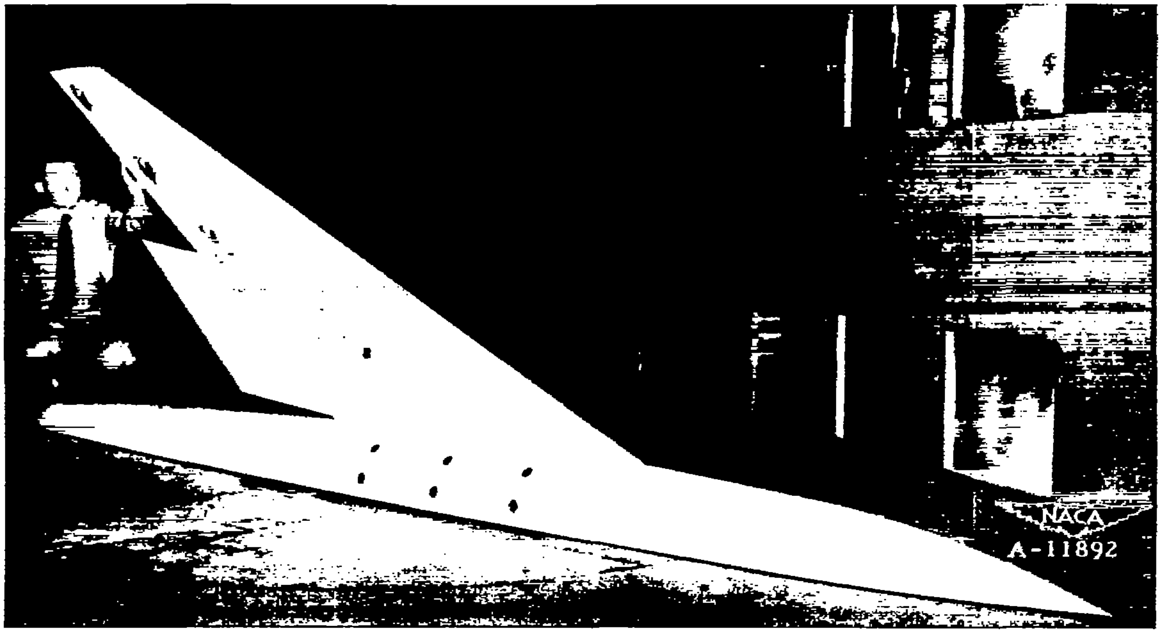
NACA
A-11892

(b) Short fuselage and split flap.

Figure 3.— The wing–fuselage combinations mounted in one of the Ames 7- by 10-foot wind tunnels.

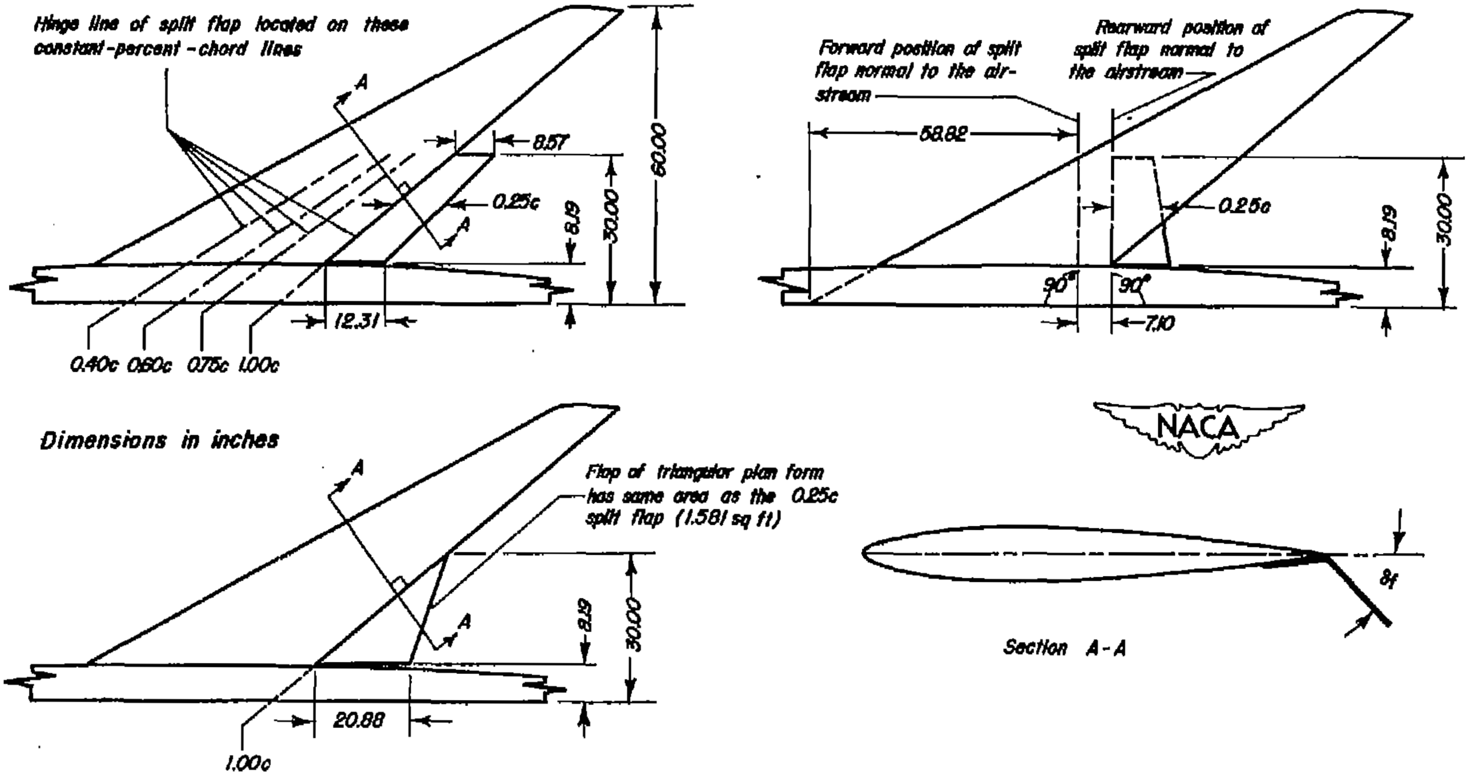
Hinge line of split flap located on these constant-percent-chord lines
A
A
8.57
0.25c
8.19
30.00
60.00
12.31
0.40c
0.60c
0.75c
1.00c
Forward position of split flap normal to the air-stream
Rearward position of split flap normal to the airstream
58.82
0.25c
8.19
30.00
90°
90°
7.10
Dimensions in inches
A
A
Flap of triangular plan form has same area as the 0.25c split flap (1.581 sq ft)
8.19
30.00
20.88
1.00c
δf
Section A-A

Figure 4.– The geometry and positions of the split flaps on the wing.

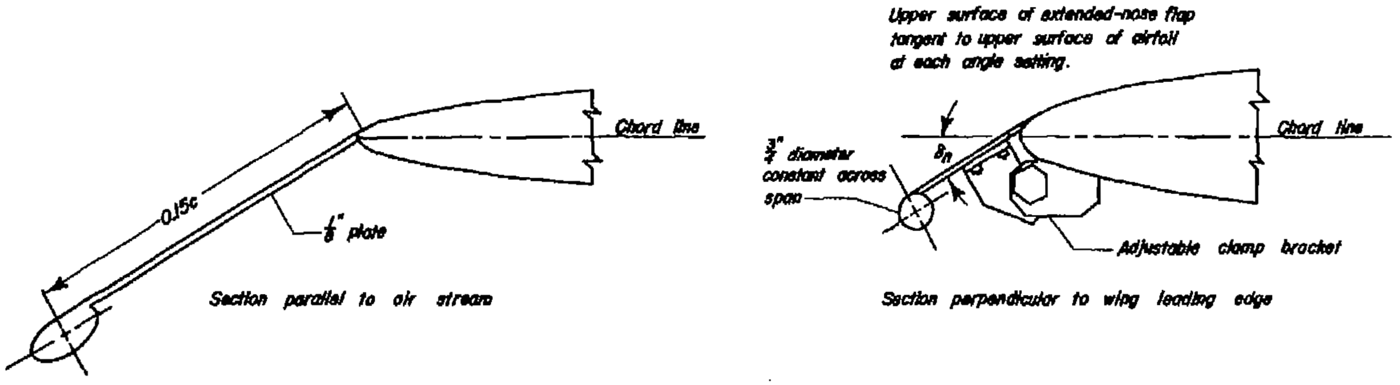
0.15c
1/8" plate
Chord line
Upper surface of extended-nose flap tangent to upper surface of airfoil at each angle setting.
3/4" diameter constant across span
δ_n
Chord line
Adjustable clamp bracket

Section parallel to air stream

Section perpendicular to wing leading edge

Extended-nose flap

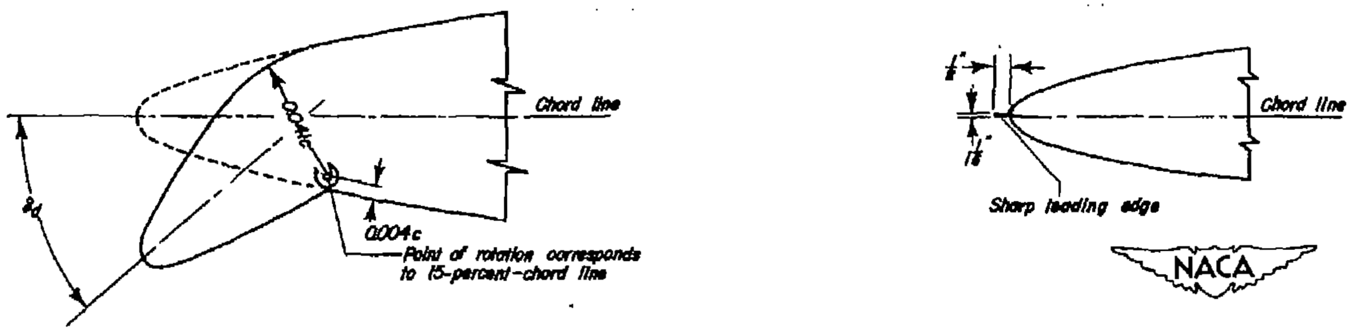
Chord line
0.04c
δ_d
0.004c
Point of rotation corresponds to 15-percent-chord line
1/8"
1/16"
Chord line
Sharp leading edge

Section perpendicular to the 15-percent chord line

Section parallel to air stream

Drooped-nose flap

Sharp leading edge

Figure 5.—The geometry of the extended-nose flap, the drooped-nose flap, and the sharp leading edge.

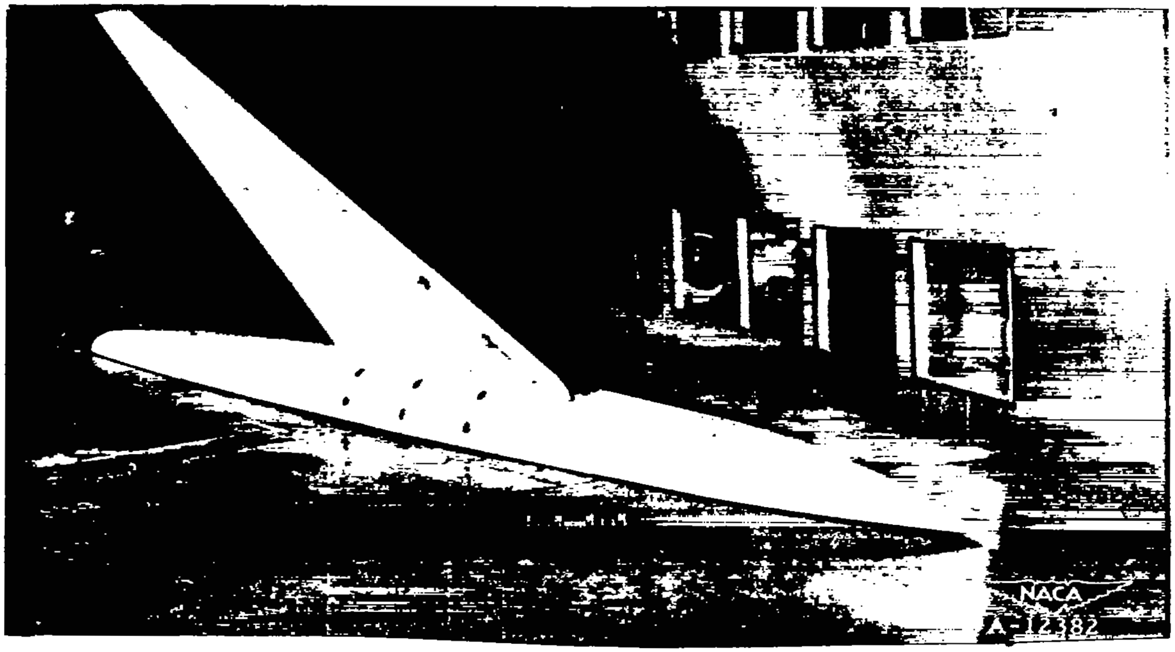
NACA
A-12382

(a) Full-span drooped-nose flap.

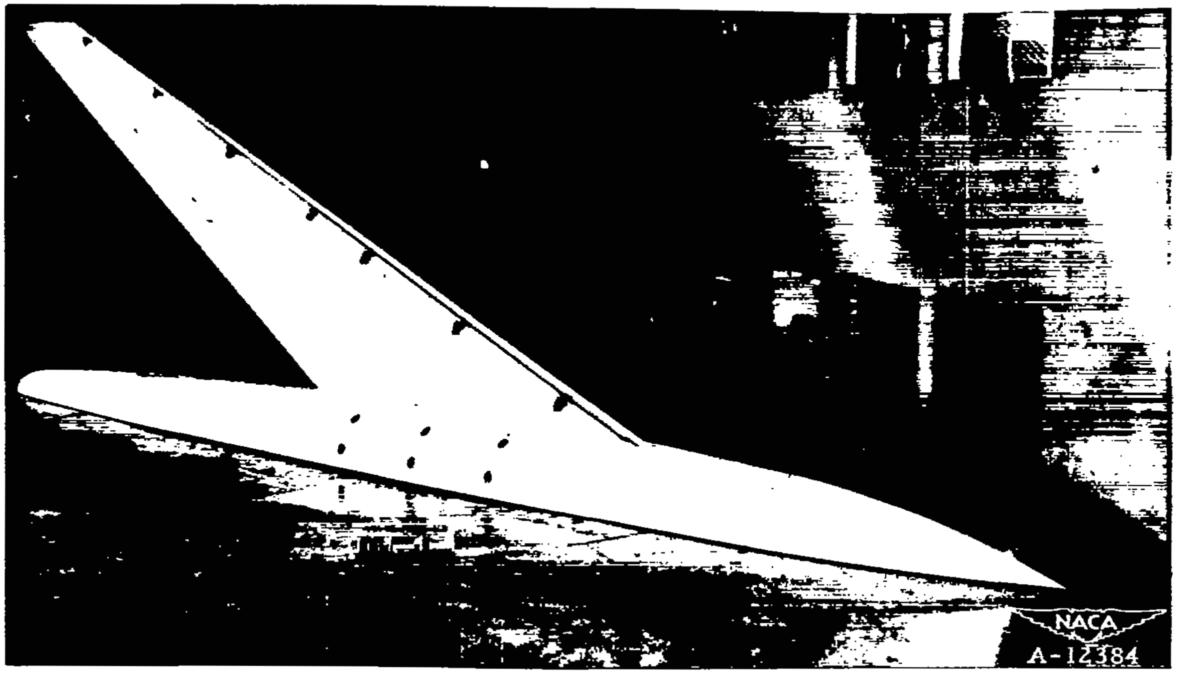
NACA
A-12384

(b) Full-span extended-nose flap.

Figure 6.- The model with leading-edge flaps mounted in one of the Ames 7- by 10-foot wind tunnels.

[redacted]

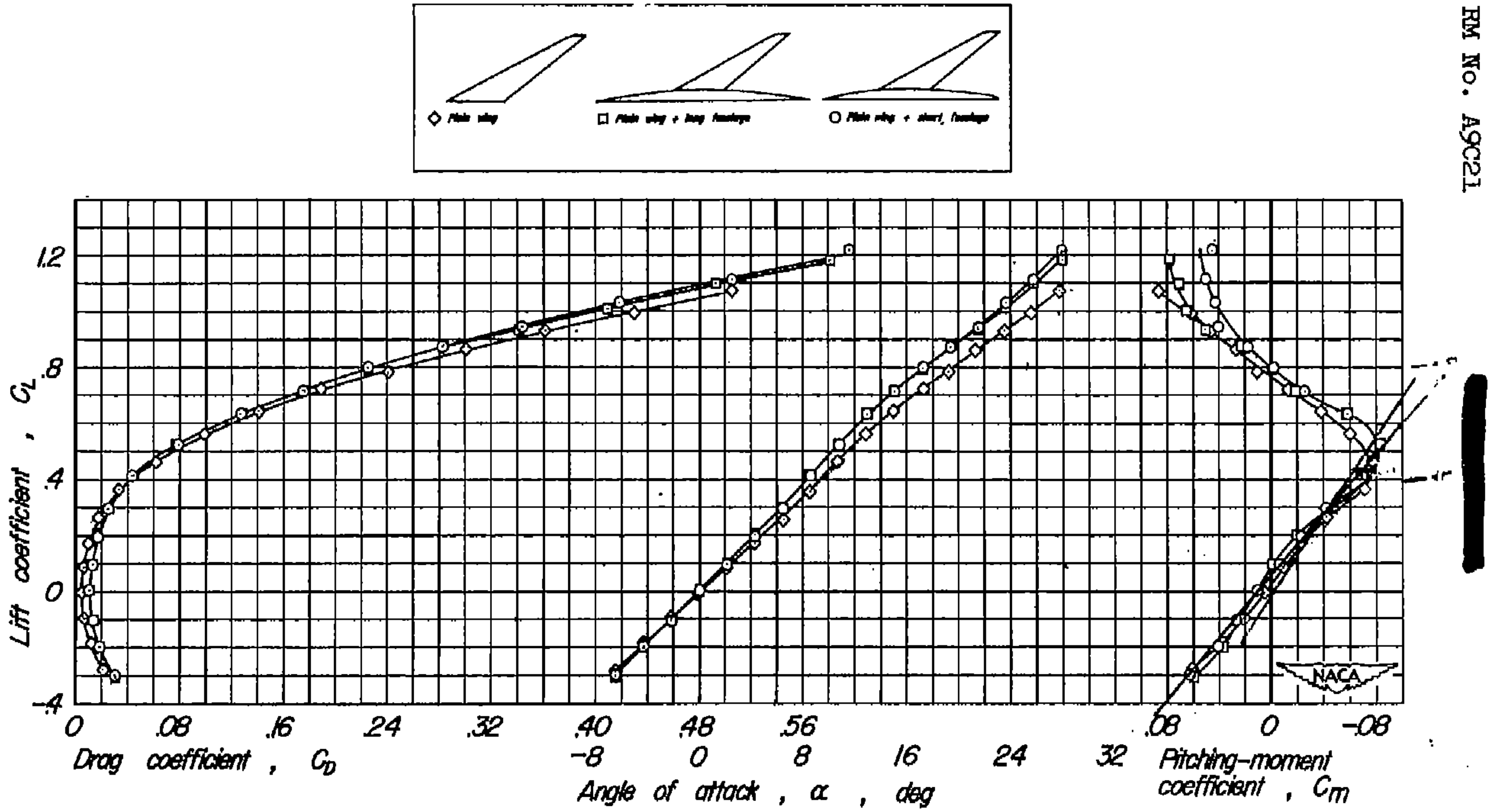

Figure 7.–Lift, drag, and pitching-moment characteristics of the plain wing and of the wing-fuselage combinations. R, 4.2 x 10⁶.

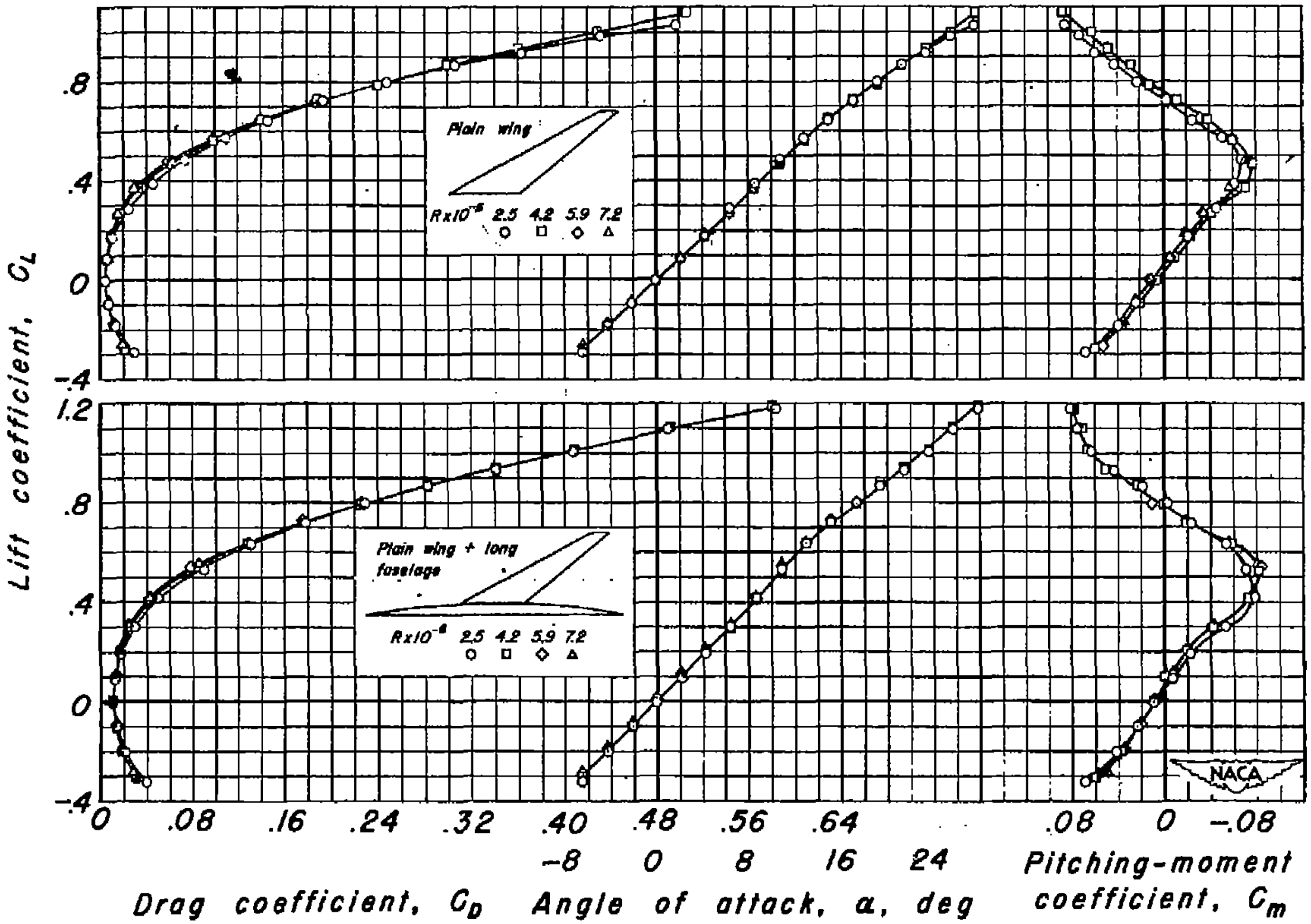

Figure 8.- Reynolds number effects on the lift, drag and pitching-moment characteristics.

[redacted]

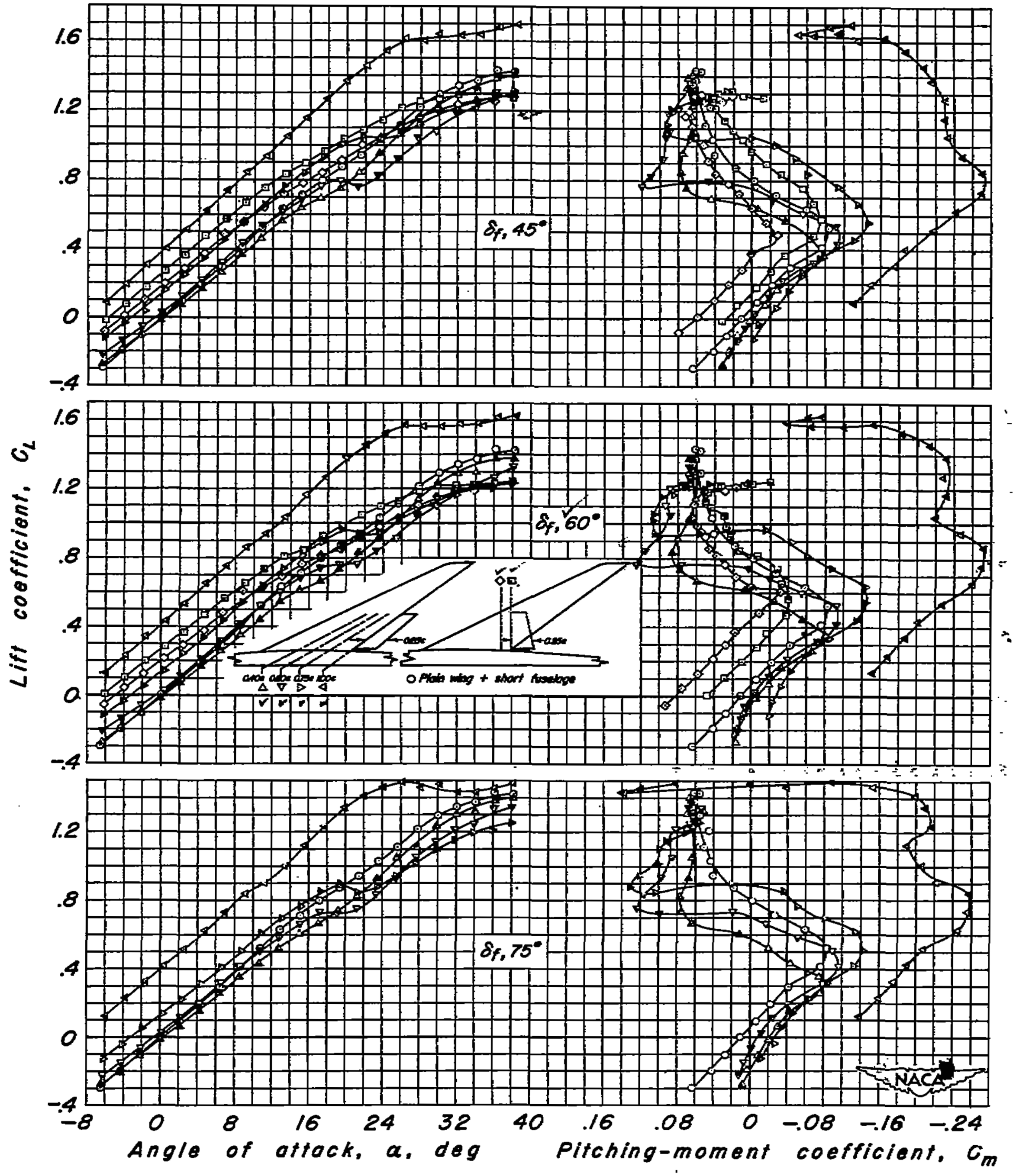

(a) C_L vs α and C_m.

Figure 9.– Effect of the split flaps in several positions on the lift, drag, and pitching-moment characteristics of the model. R, 4.2×10^6.

[redacted]

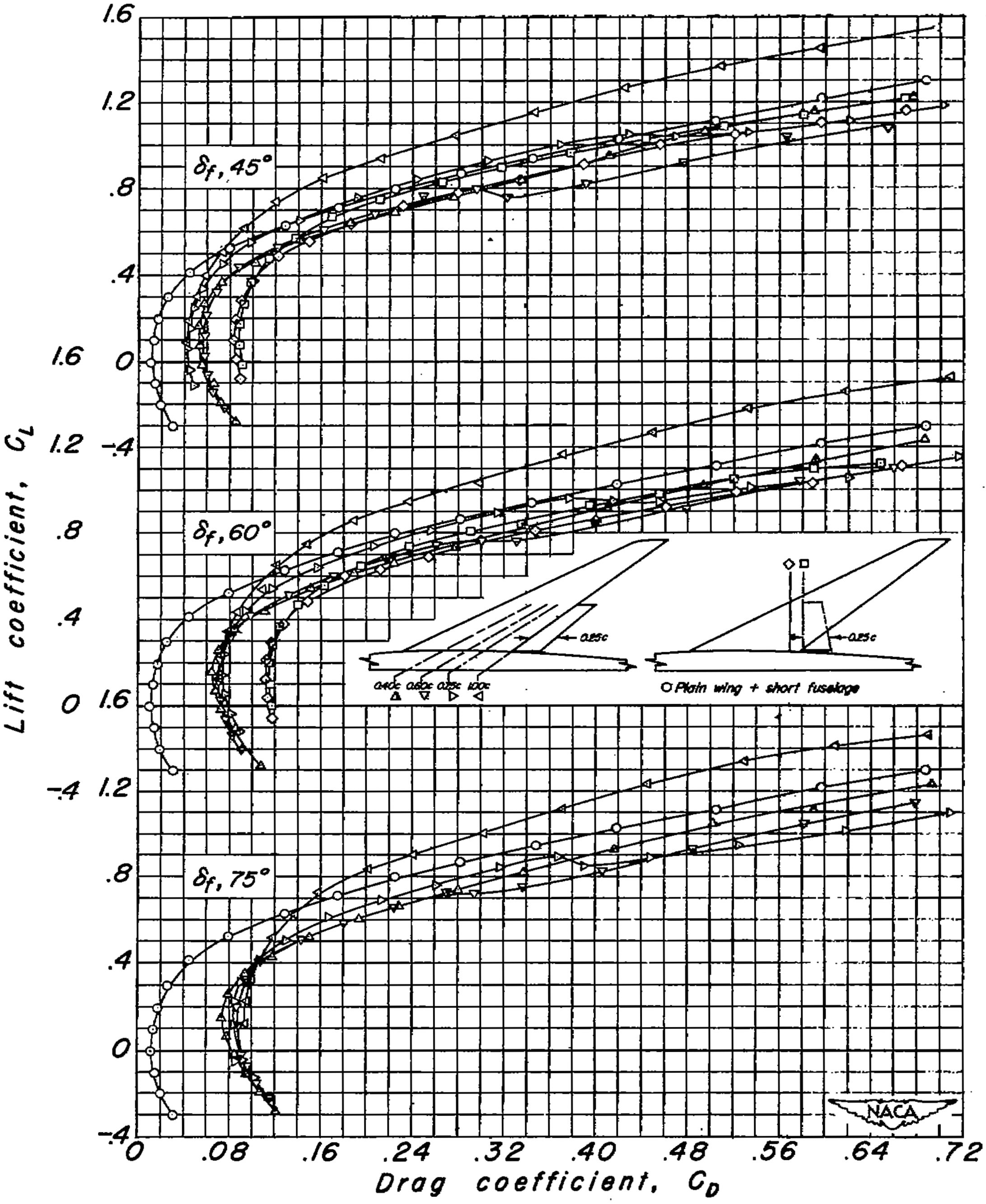

(b) C_L vs C_D.

Figure 9.- Concluded.

[redacted]

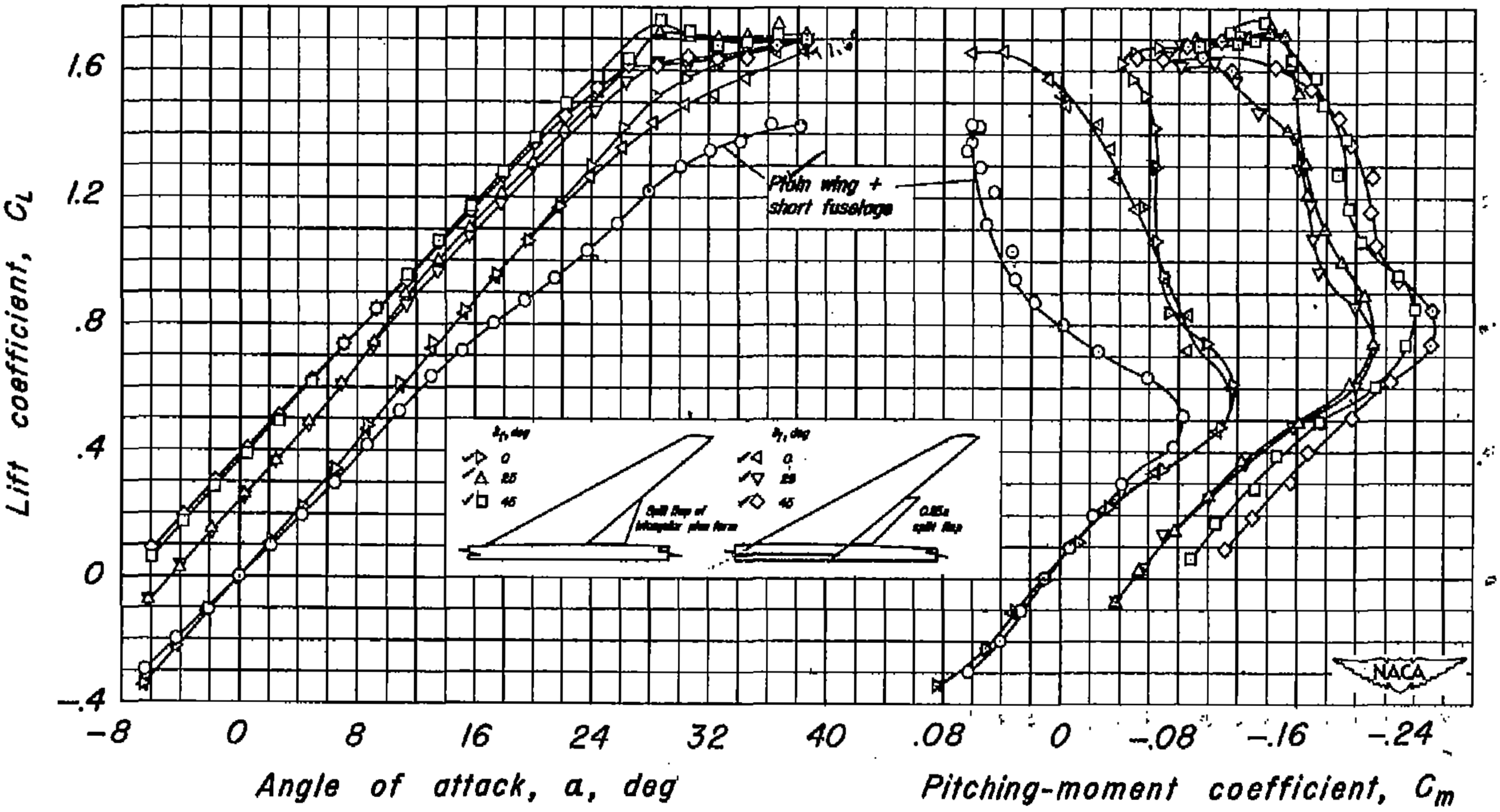

(a) C_L vs α and C_m.

Figure 10.– Effect of the split flaps of different plan forms on the lift, drag, and pitching-moment characteristics of the model. R, 4.2 x 10^6.

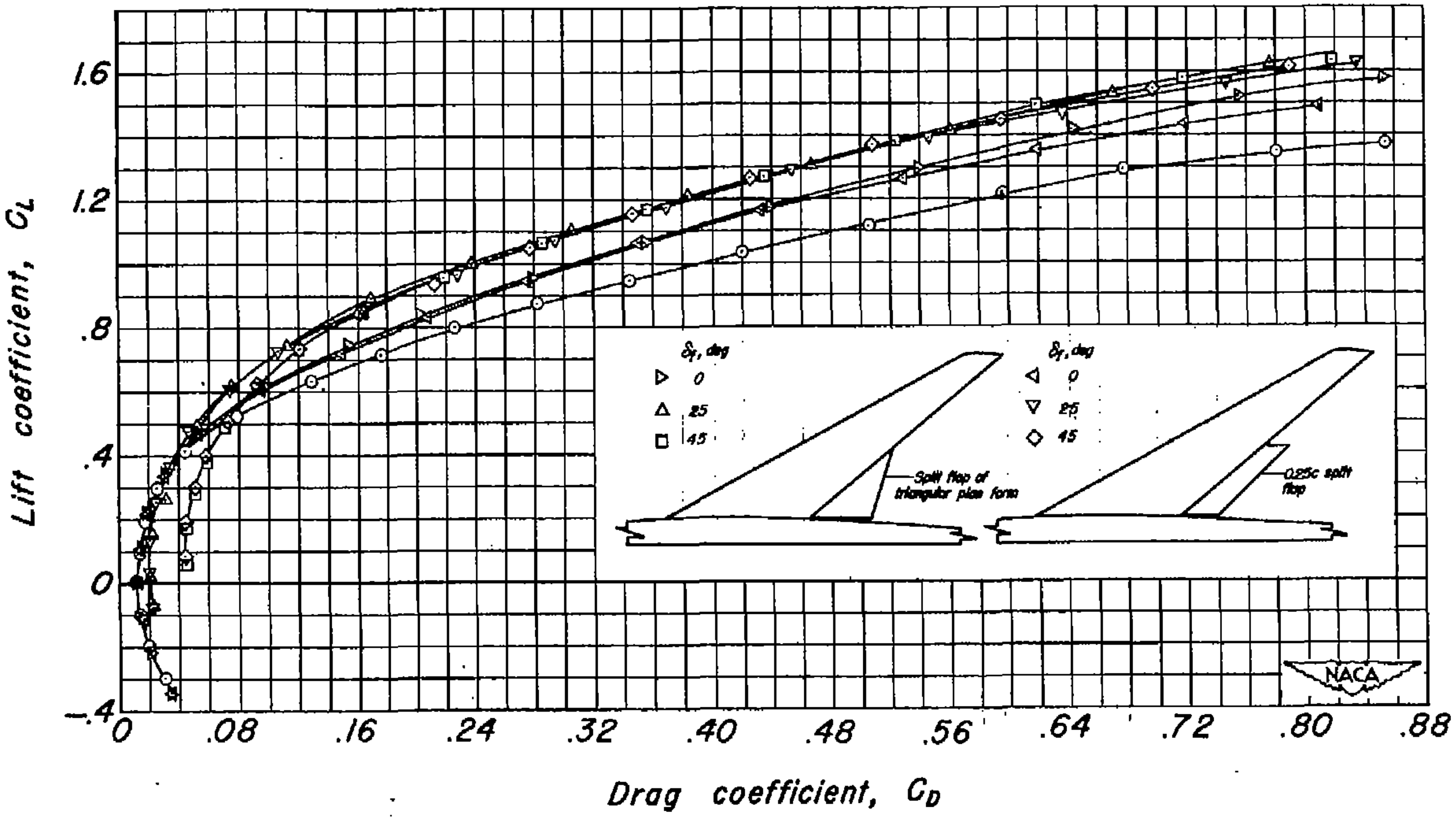

(b) C_L vs C_D.

Figure 10.– Concluded.

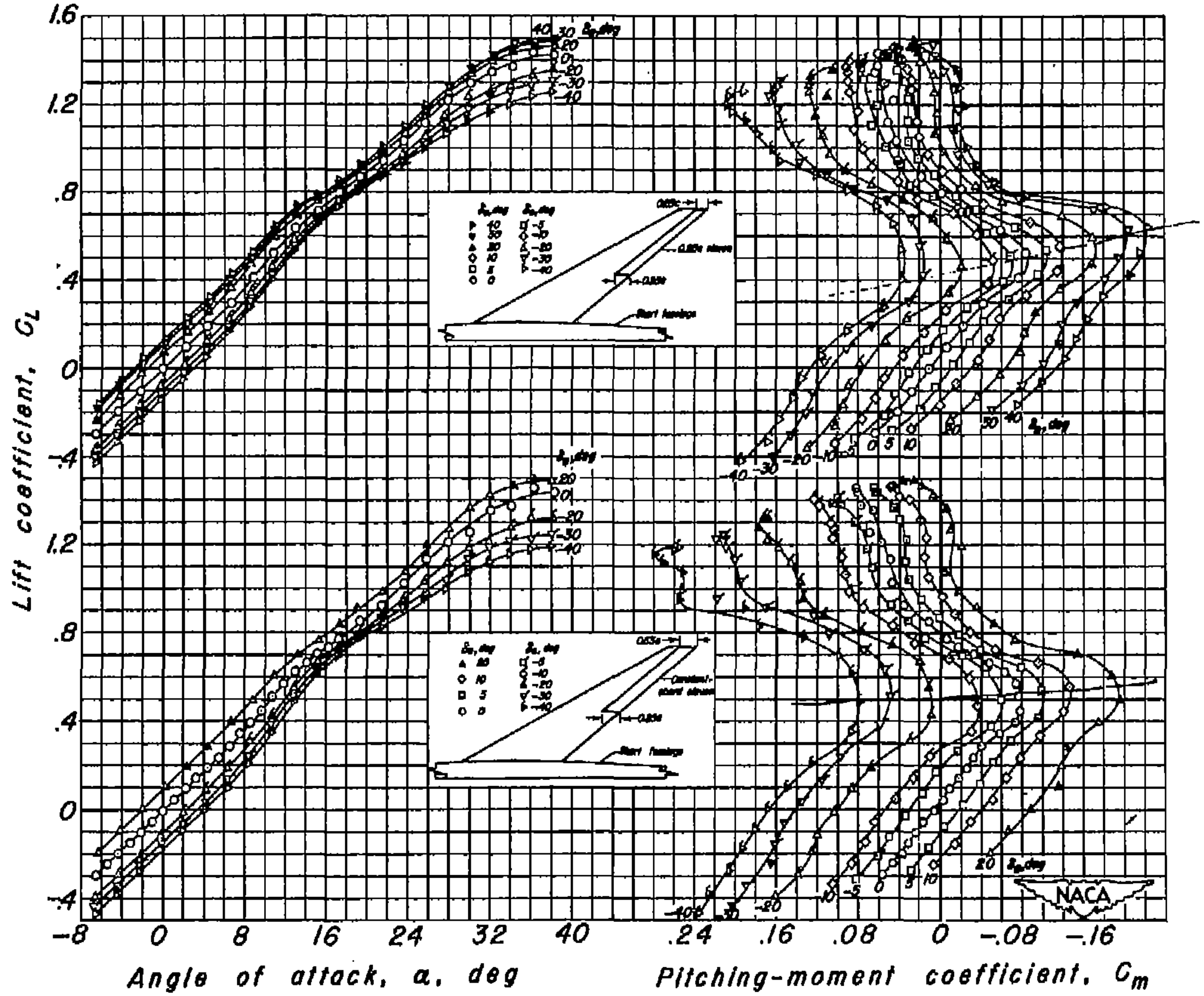

(a) C_L vs α and C_m.

Figure 11.- Comparative effectiveness of the 25-percent chord elevon and the constant-chord elevon. R, 4.2 x 10^6.

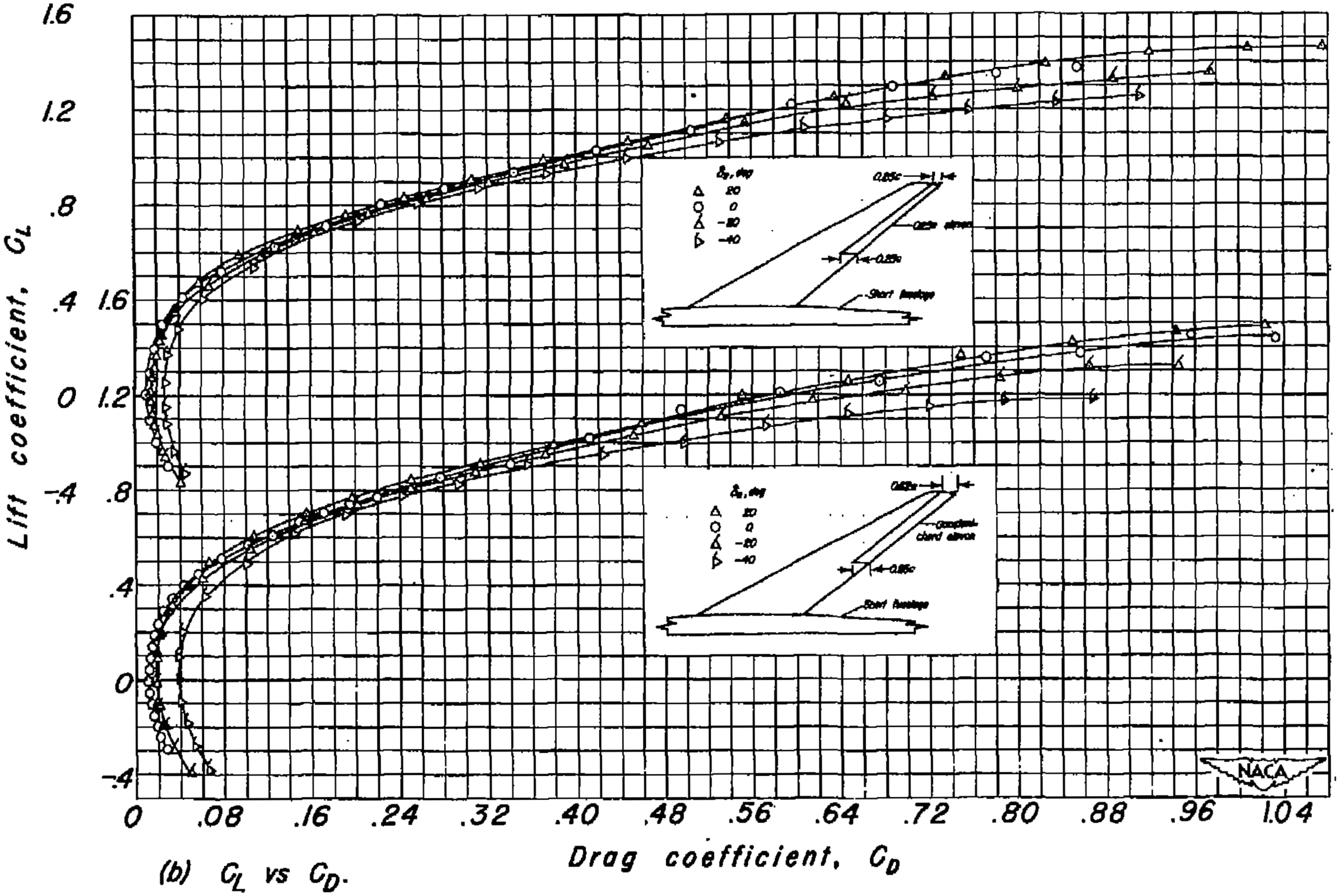

(b) C_L vs C_D.

Figure 11.- Continued.

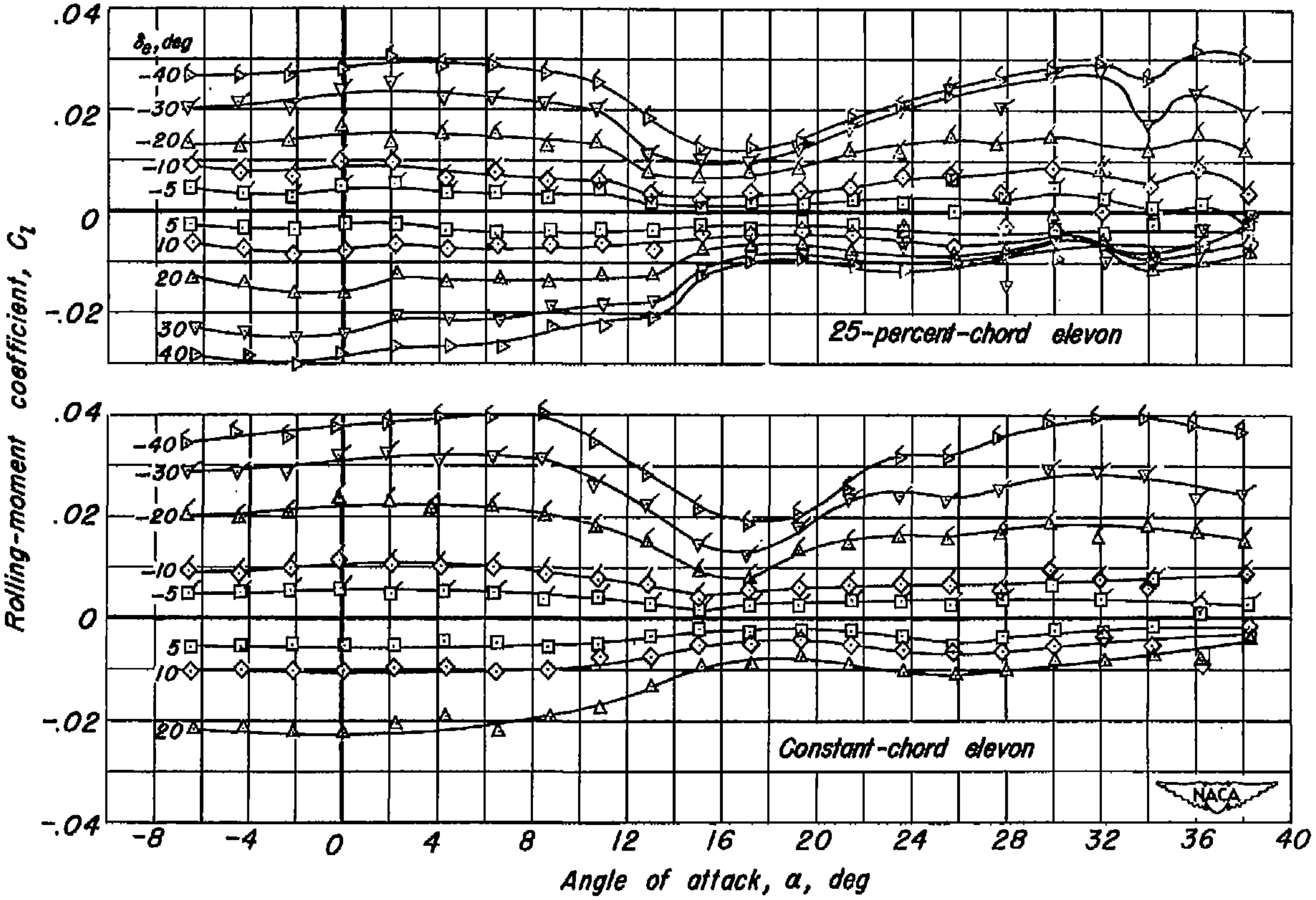

(c) C_l vs α.

Figure 11.- Concluded.

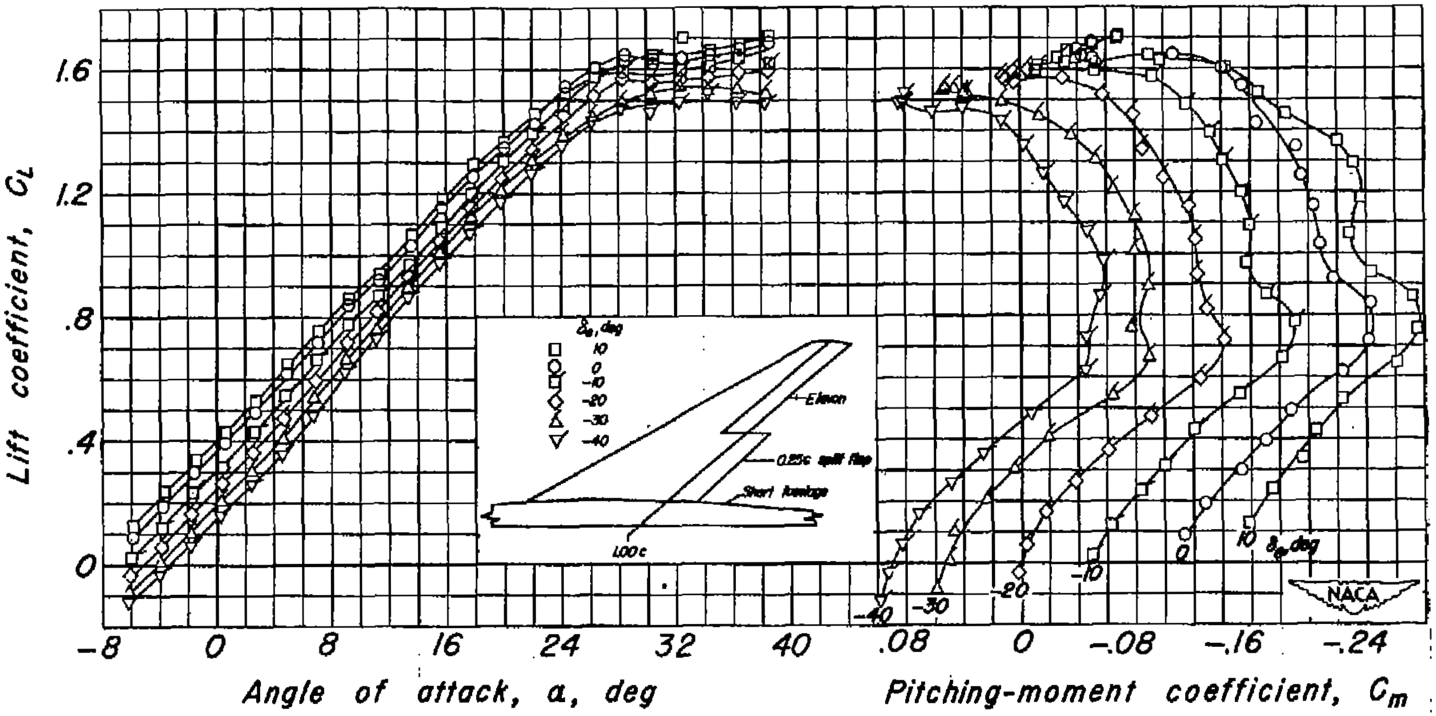

(a) C_L vs α and C_m.

Figure 12.- Effectiveness of the constant-chord elevon with the split flap deflected 45°. R, 4.2×10^6.

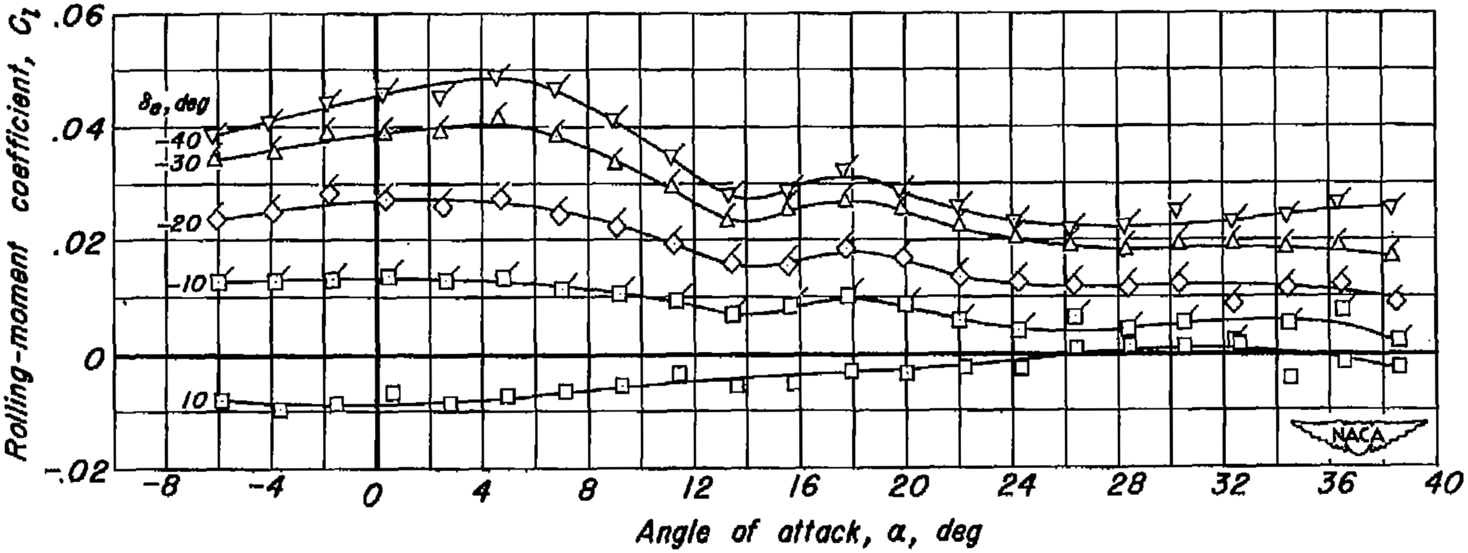

(b) C_l vs α.

Figure 12.- Concluded.

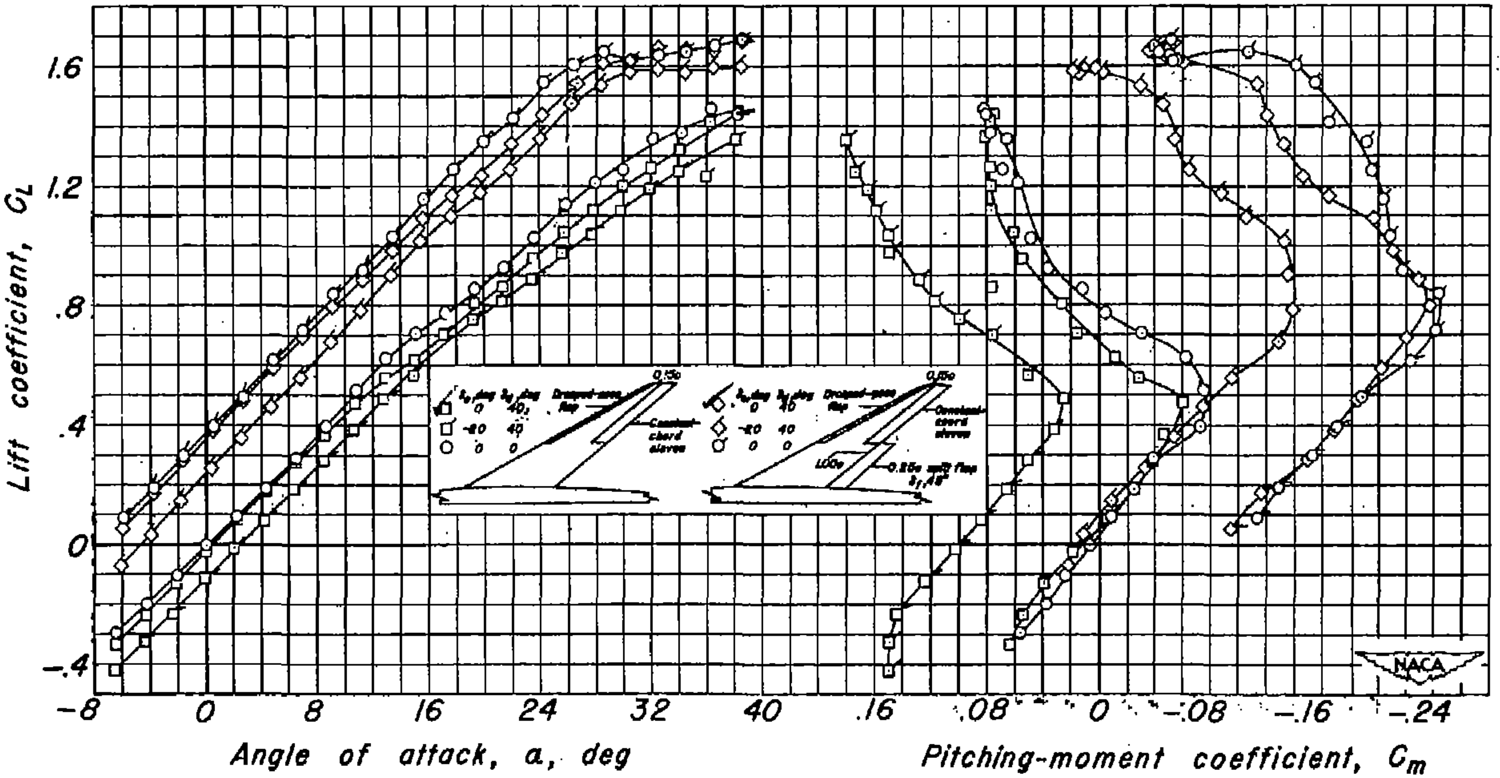

Figure 13.- Effect of the drooped-nose flap of 50-percent span on the lift and pitching-moment characteristics of the model with short fuselage. R, 4.2x10⁶.

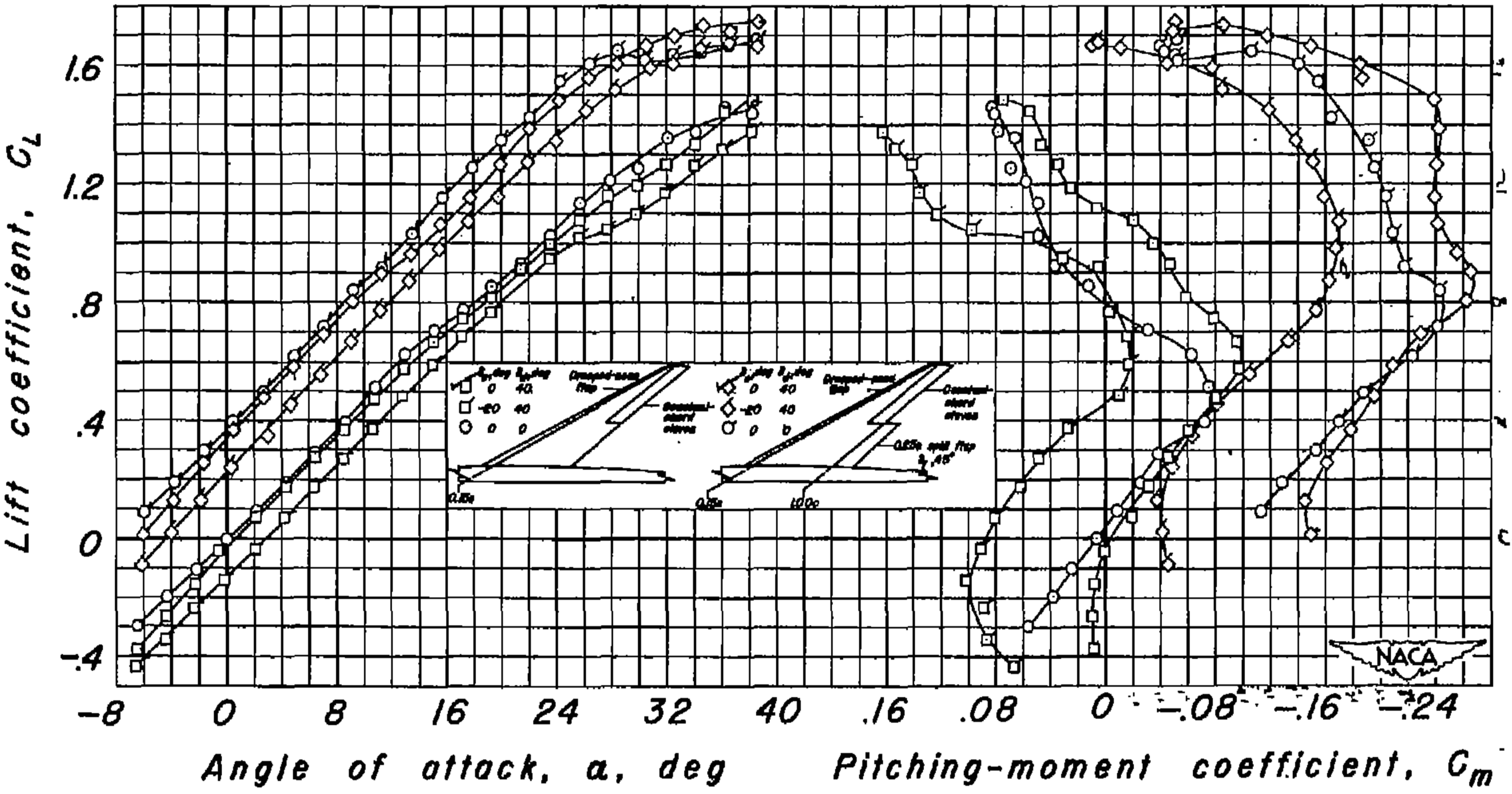

Figure 14.– Effect of the drooped-nose flap of full span on the lift and pitching-moment characteristics of the model with short fuselage. R, 4.2×10^6.

2

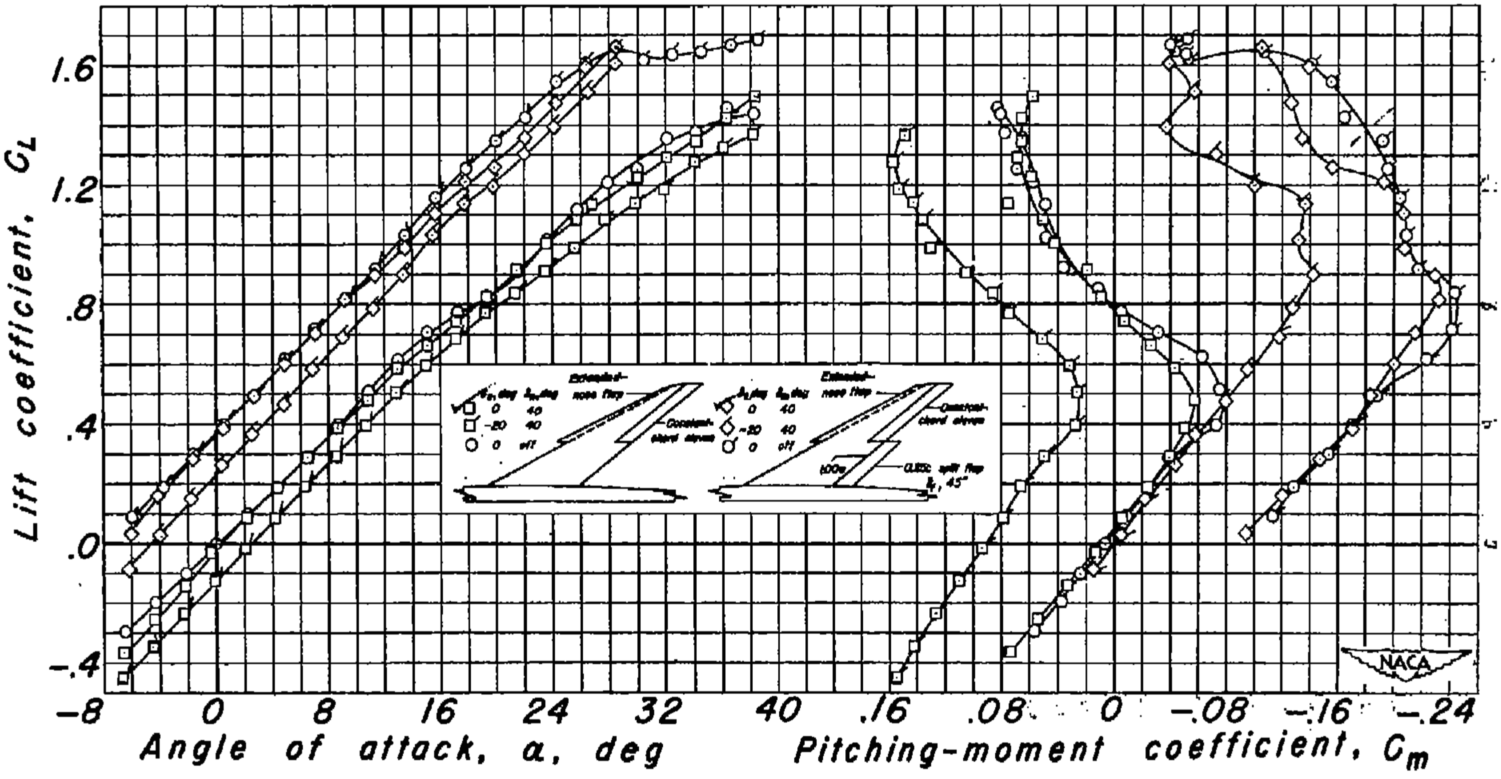

Figure 15.- Effect of the extended-nose flap of 50-percent span on the lift and pitching-moment characteristics of the model with short fuselage. R, 4.2 x 10^6.

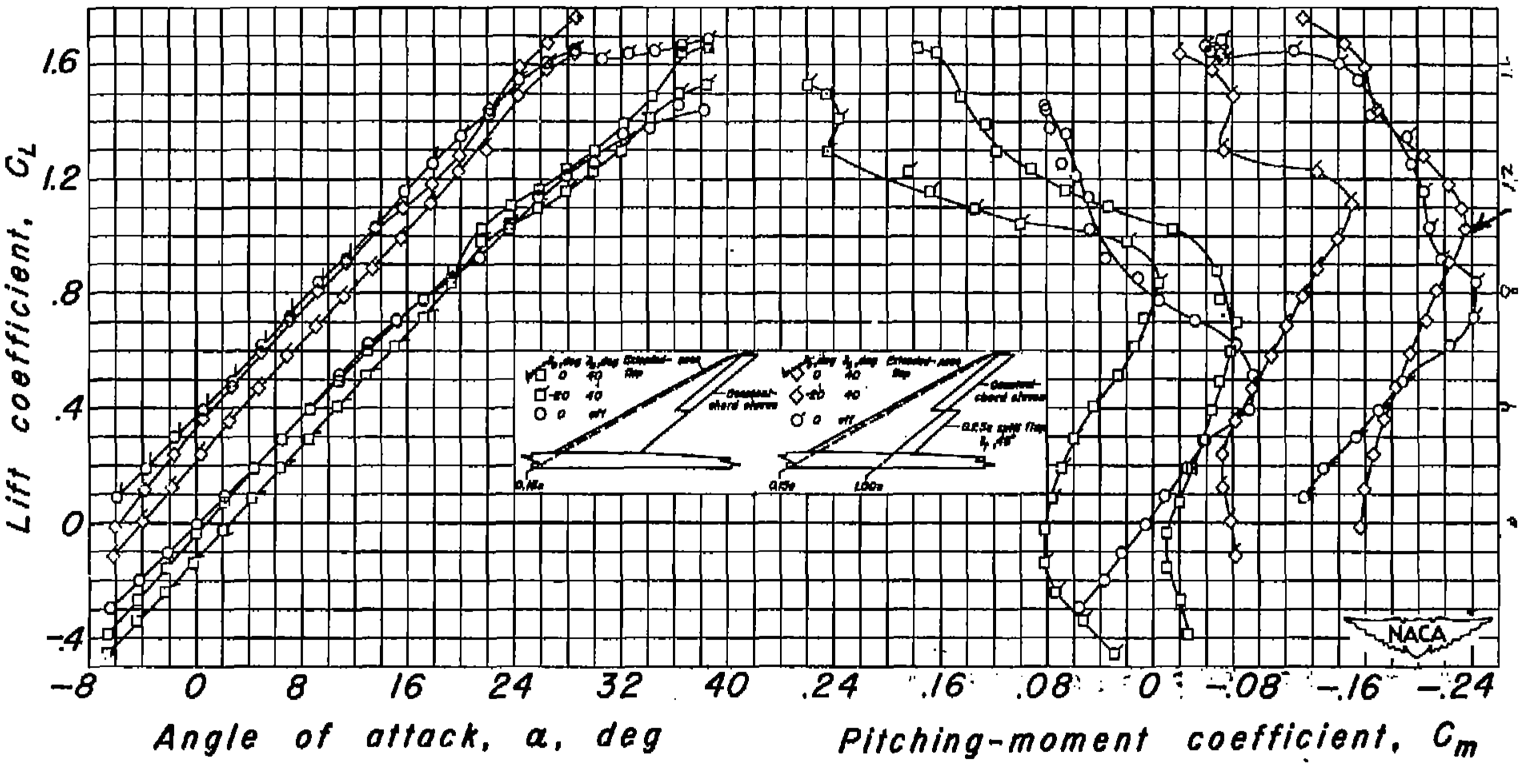

Figure 16.– Effect of the extended-nose flap of full span on the lift and pitching-moment characteristics of the model with short fuselage. R,4.2x10⁶

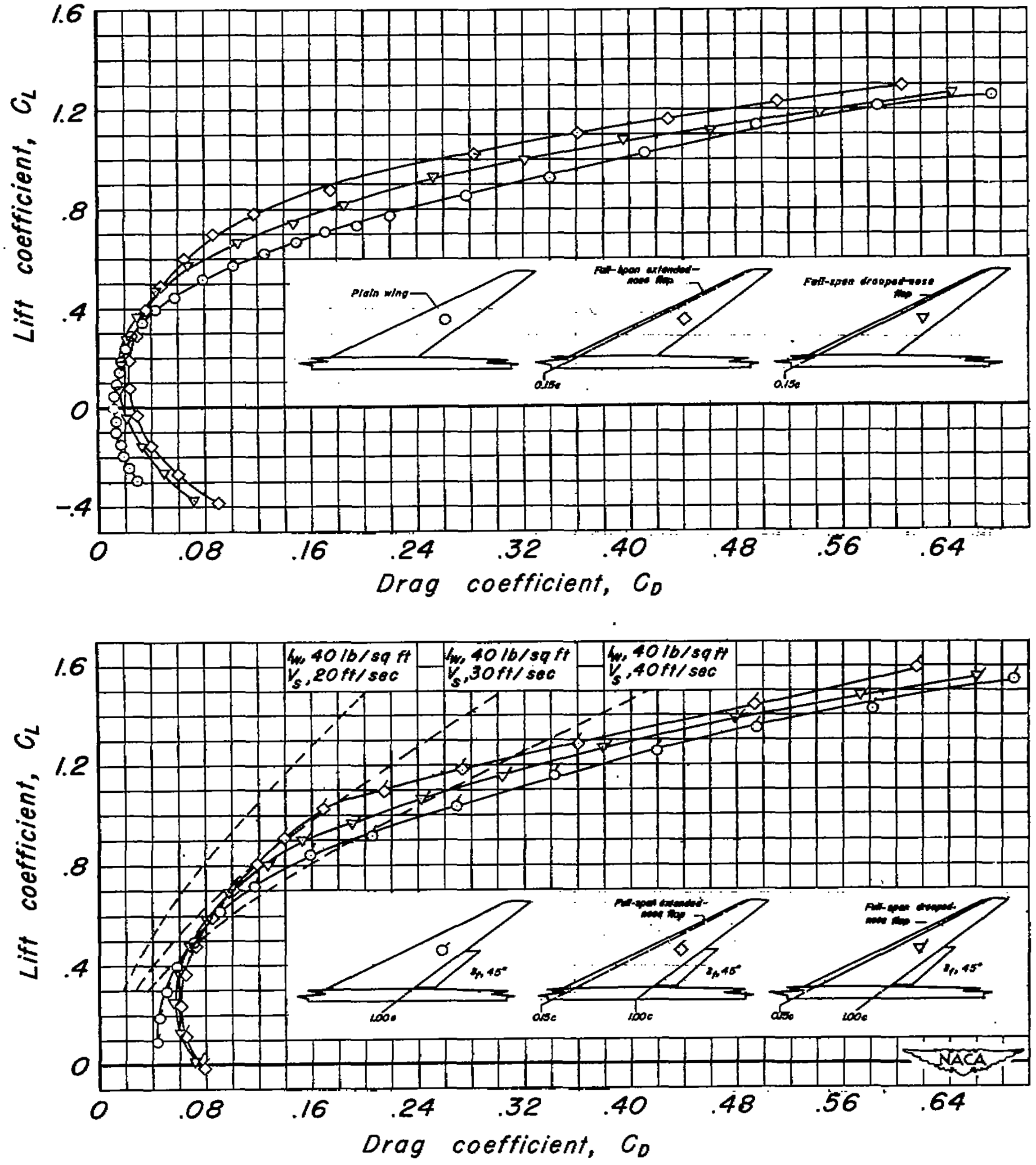

Figure 17– Effect of the drooped-nose flap and the extended-nose flap of full span on the drag characteristics of the model with short fuselage. R, 4.2 x 10⁶.

[redacted]

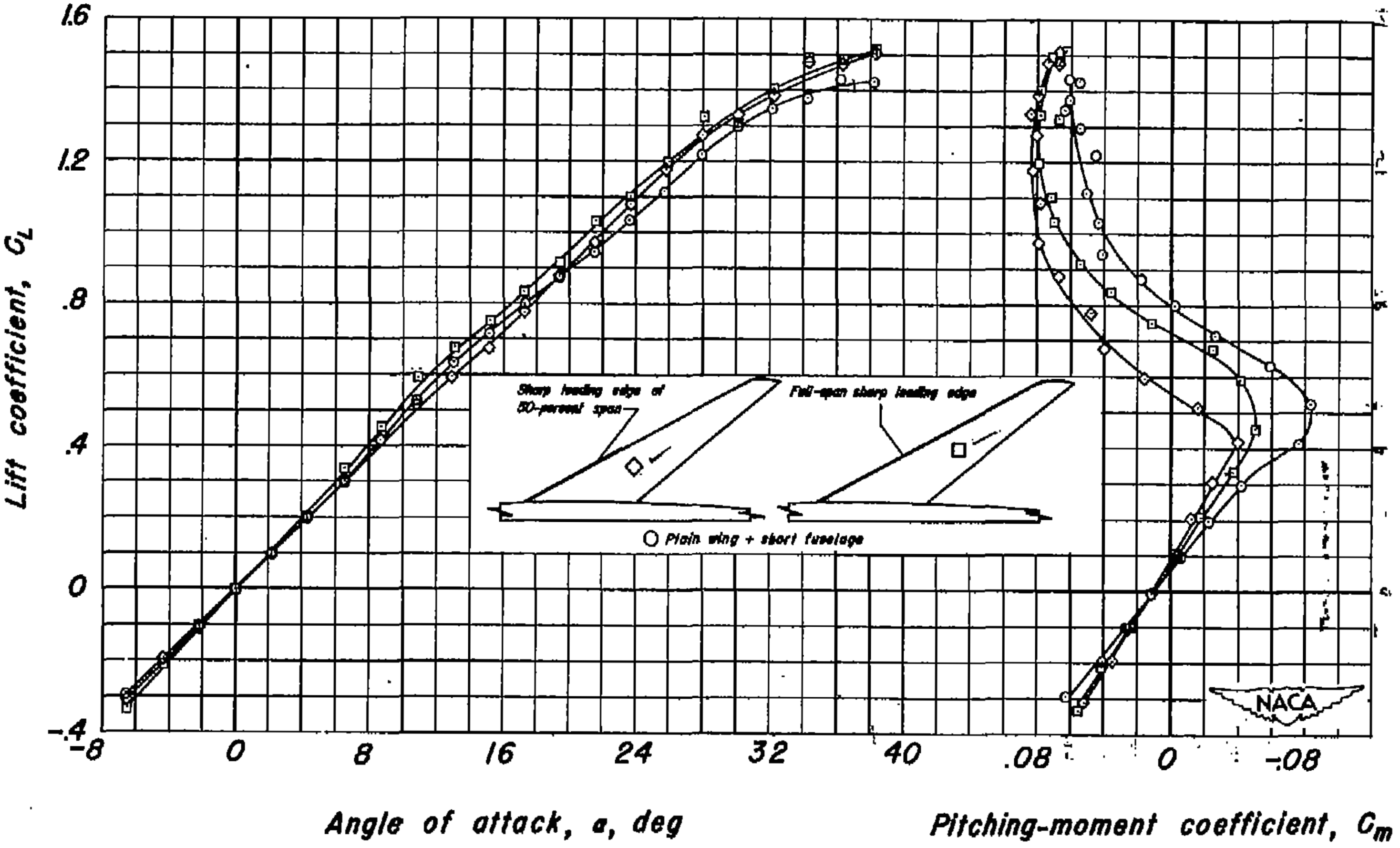

(a) C_L vs α and C_m.

Figure 18.- Effect of sharp leading edges on the lift, drag, and pitching-moment characteristics of the model. $R, 4.2 \times 10^6$.

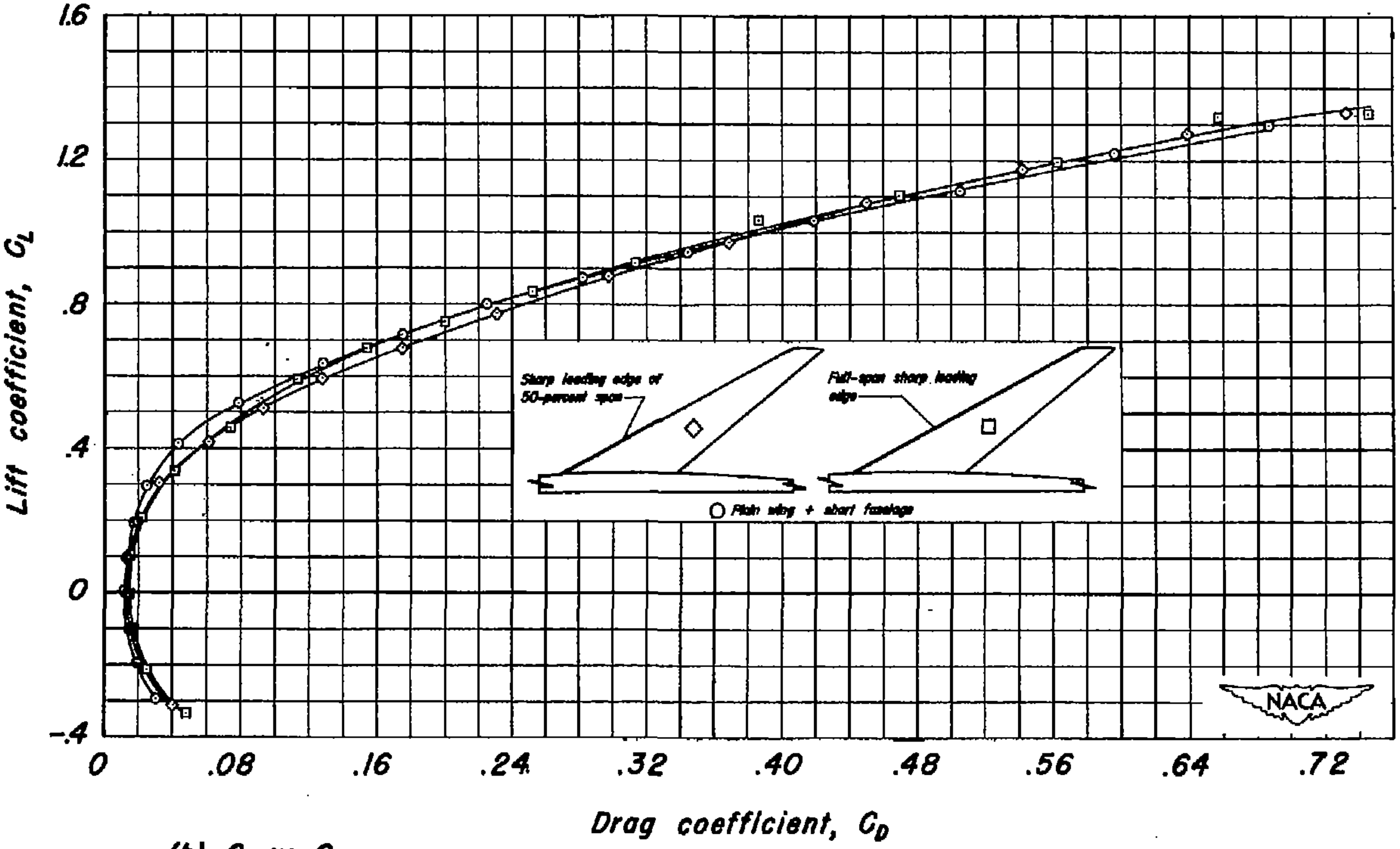

(b) C_L vs C_D.

Figure 18.- Concluded.

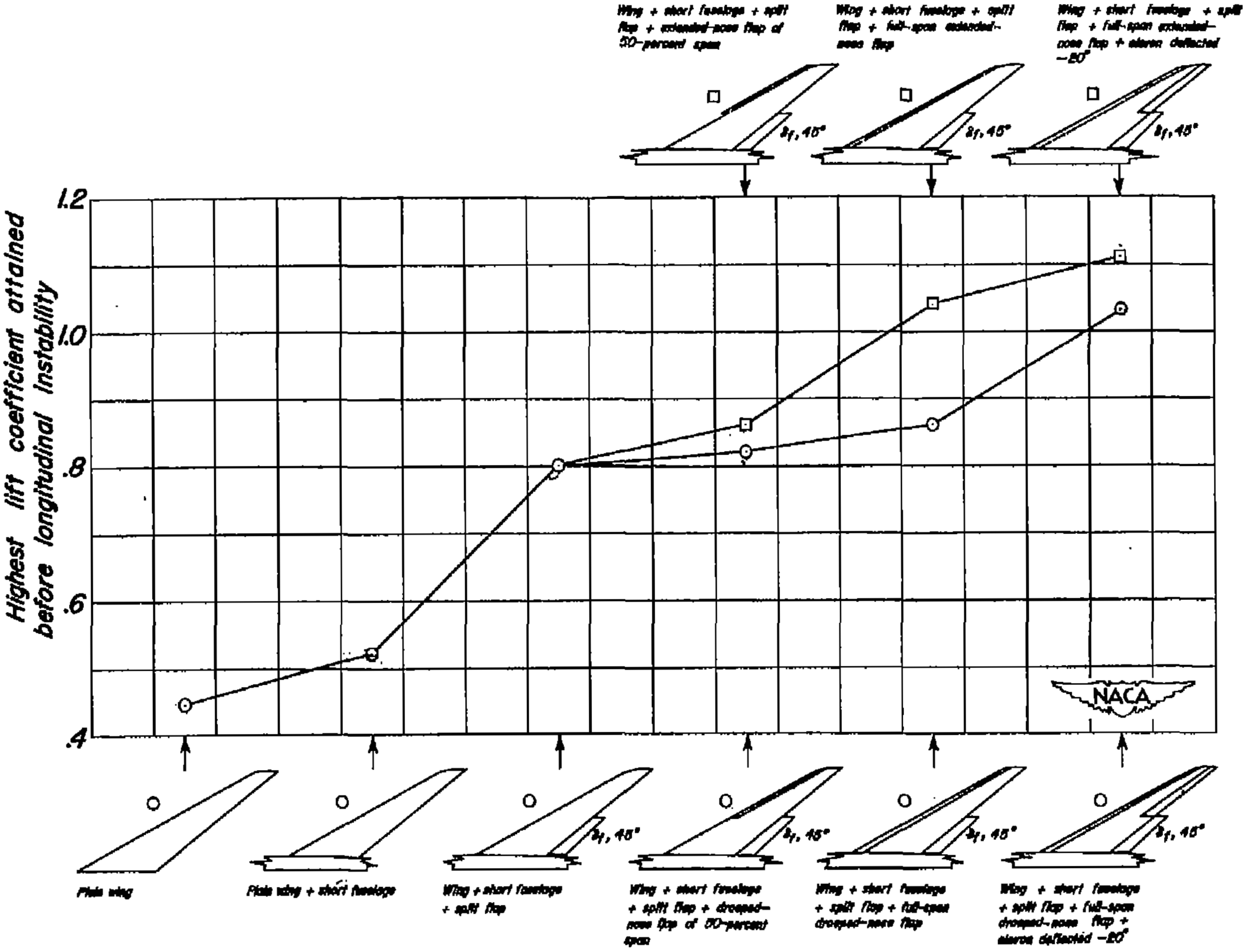

Figure 19.– Effect of the fuselage and flap changes on the highest lift coefficient attained before the occurrence of longitudinal instability. R, 4.2×10^6.

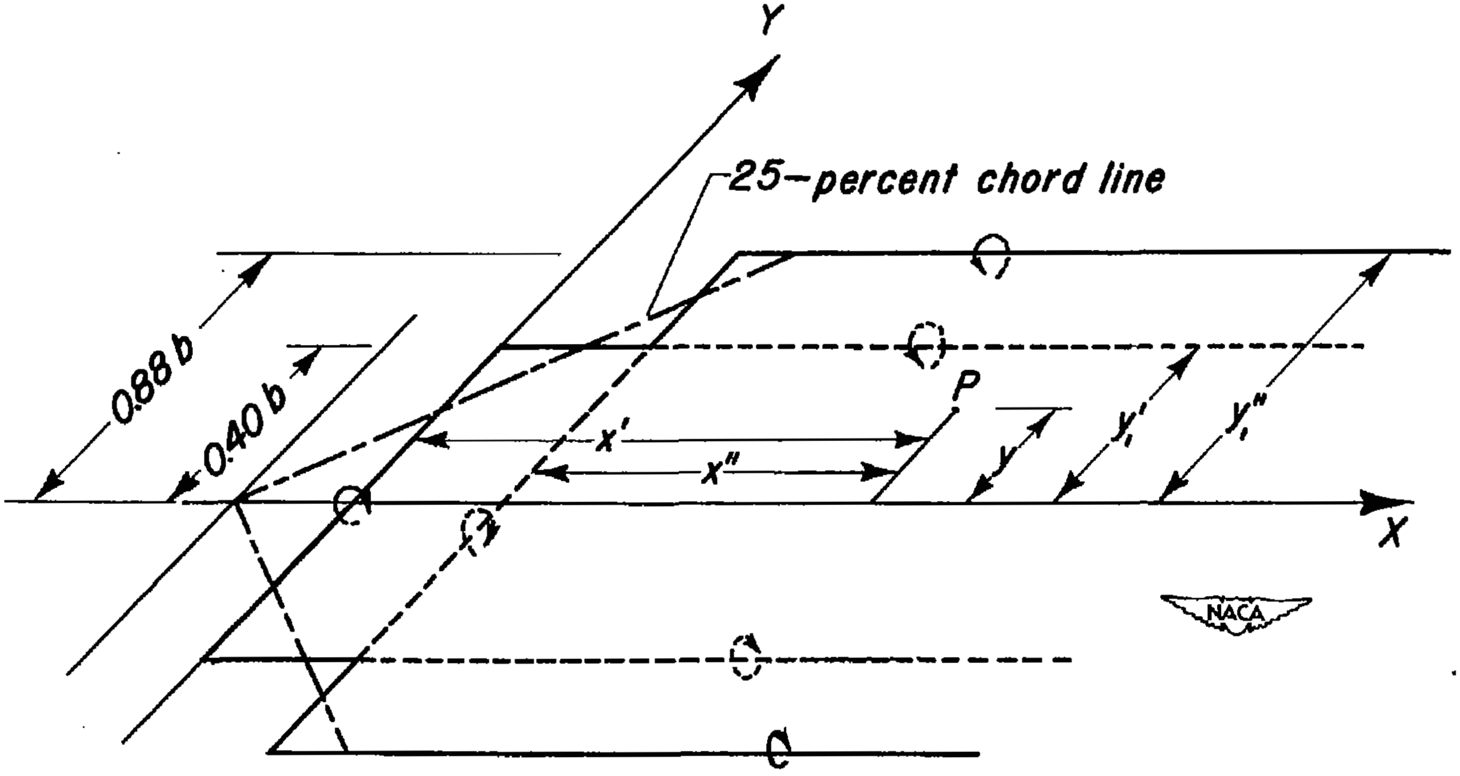
Y
25-percent chord line
0.88 b
0.40 b
P
x'
x''
y
y_1'
y_1''
X

Figure 20.- The staggered horseshoe vortex system.

NASA Technical Library
3 1176 01434 4742